

D4.5 MESMER-L-X
climate feedback
emulator at the
service of EU forest
policy modelling

Emulating local direct temperature change induced by forest changes





<b>Grant Agreement</b>	101056875
Call identifier	HORIZON-CL5-2021-D1-01
Project full title	ForestNavigator: Navigating European forests and forest bioeconomy sustainably to EU climate neutrality
Work package	WP4
<b>Due date</b>	30/06/2025
Deliverable lead	Ludwig-Maximilians-Universität
Authors	Meri Räty (LMU), Yi Yao (ETH), Julia Pongratz (LMU), Sonia I. Seneviratne

### **Abstract**

This report describes the development of the MESMER-L-X emulator. We analyzed multiple COSMO-CLM² regional climate model simulations under different forest scenarios, which provided the foundation for developing an emulator that accurately predicts local direct temperature effects from forest changes. The tool successfully reproduces key outcomes from the original climate simulations and offers a fast and reliable method of assessing climate impacts related to different forest management strategies and has further potential for extension with additional simulation datasets. This capability will be harnessed to support European forest policy pathways modelling.

### **Keywords**

Biogeophysical effects, forest management, emulator

Internal Technical Auditor	Name (Beneficiary short name)	Date of approval
Task leader	Julia Pongratz (LMU)	23/07/2025
WP leader	Julia Pongratz (LMU)	23/07/2025
Coordinators	Petr Havlík and Fulvio Di Fulvio (IIASA)	22/07/2025
Project Office	Eleonora Tan (IIASA)	23/07/2025

This report reflects only the authors' view, and the Agency is not responsible for any use that may be made of the information it contains.

### **Dissemination level**

**PU** Public, will be published on CORDIS

**SEN** Sensitive, limited under the conditions of the Grant Agreement



Nature of the deliverable \*

K



# **Table of Contents**

	Abstract	
	Dissemination level	2
List	of Figures	4
List	of Tables	5
Abb	previations	6
Exe	cutive summary	7
1.	Introduction	8
2.	Forest scenarios simulated with COSMO-CLM <sup>2</sup>	9
2.1.	Simulation setup	9
2.2.	Modelled biophysical responses	12
	2.2.1. Afforestation	
	2.2.2. Deforestation	
	2.2.3. Conversion from needleleaf to broadleaf	
	2.2.4. Conversion from broadleaf to needleleaf	16
3.	Development of the MESMER-L-X Emulator	18
3.1.	Formulation of the emulator equations	18
3.2.	Statistical relationships between forest type changes and temperature variables	18
	3.2.1. Afforestation	18
	3.2.2. Deforestation	
	3.2.3. Conversion to broadleaf forests	
	3.2.4. Conversion to coniferous forests	26
4.	Challenges and prospects for incorporating ICON-ESM Simulatio	ns into
	MESMER-L-X	29
5.	Discussion	33
6.	Conclusion	34
7.	References	35
8.	Annexes	38
8.1.	Manual of the emulator	
8.2.	Description of the appendix netCDF files	39



# **List of Figures**

Figure 1. Sub-grid cell level structure of the Community Land Model version 5	10
Figure 2. Visual example of the separation process of direct and indirect impacts	11
Figure 3. Direct biogeophysical impacts of the conversion from grassland to forests on average (2025)	5-2074)
monthly mean daily maximum temperature (in K)	
Figure 4. Indirect biogeophysical impacts of the conversion from grassland to forests on average (2025)	5-2074)
monthly mean daily maximum temperature (in K)	
Figure 5. Direct biogeophysical impacts of the conversion from forests to grassland on average (2025)	5-2074)
monthly mean daily maximum temperature (in K)	
Figure 6. Indirect biogeophysical impacts of the conversion from forests to grassland on average (2025)	
monthly mean daily maximum temperature (in K)	
Figure 7. Direct biogeophysical impacts of the conversion from coniferous forests to broadleaf forests on a	
(2025-2074) monthly mean daily maximum temperature (in K)	
Figure 8. Indirect biogeophysical impacts of the conversion from coniferous forests to broadleaf forests.	
average (2025-2074) monthly mean daily maximum temperature (in K)	
Figure 9. Direct biogeophysical impacts of the conversion from broadleaf forests to coniferous forests on a	_
(2025-2074) monthly mean daily maximum temperature (in K)	
Figure 10. Indirect biogeophysical impacts of the conversion from broadleaf forests to coniferous fore	
average (2025-2074) monthly mean daily maximum temperature (in K)	
Figure 11. Slope of the linear relationship between direct biogeophysical impacts of the conversion	
grassland to forests on monthly mean daily maximum temperature and the temperature of the grid-cell	
Figure 12. Standard deviation of the residual calculated based on the linear relationship between	
biogeophysical impacts of the conversion from grassland to forests on monthly mean daily ma	
temperature and the temperature of the grid-cell	
Figure 13. R-squared value of the linear relationship between direct biogeophysical impacts of the converse desired to the con	
from grassland to forests on monthly mean daily maximum temperature and the temperature of the grid-	
Figure 14. P-value of the linear relationship between direct biogeophysical impacts of the conversion	
grassland to forests on monthly mean daily maximum temperature and the temperature of the grid-cell	
Figure 15. Slope of the linear relationship between direct biogeophysical impacts of the conversion from	
to grassland on monthly mean daily maximum temperature and the temperature of the grid-cell	
Figure 16. Standard deviation of the residual calculated based on the linear relationship between biogeophysical impacts of the conversion from forests to grassland on monthly mean daily ma	
temperature and the temperature of the grid-cell	
Figure 17. R-squared value of the linear relationship between direct biogeophysical impacts of the conv	
from forests to grassland on monthly mean daily maximum temperature and the temperature of the grid-	
Figure 18. P-value of the linear relationship between direct biogeophysical impacts of the conversion from	
to grassland on monthly mean daily maximum temperature and the temperature of the grid-cell	
Figure 19. Slope of the linear relationship between direct biogeophysical impacts of the conversion	
coniferous forests to broadleaf forests on monthly mean daily maximum temperature and the temperature	
grid-cellgrid-cell	
Figure 20. Standard deviation of the residual calculated based on the linear relationship between	
biogeophysical impacts of the conversion from coniferous forests to broadleaf forests on monthly mea	
maximum temperature and the temperature of the grid-cell	
Figure 21. R-squared value of the linear relationship between direct biogeophysical impacts of the conv	
from coniferous to broadleaf forests on monthly mean daily maximum temperature and the temperature	
grid-cell	
Figure 22. P-value of the linear relationship between direct biogeophysical impacts of the conversion	
coniferous to broadleaf forests on monthly mean daily maximum temperature and the temperature of the	
cell	_
Figure 23. Slope of the linear relationship between direct biogeophysical impacts of the conversion	
broadleaf to coniferous forests on monthly mean daily maximum temperature and the temperature of the	
cell	_
Figure 24. Standard deviation of the residual calculated based on the linear relationship between	direct
biogeophysical impacts of the conversion from broadleaf to coniferous forests on monthly mean daily ma	ximum
temperature and the temperature of the grid-cell	27



Figure 25. R-squared value of the linear relationship between direct biogeophysical impacts of the conversion from broadleaf to coniferous forests on monthly mean daily maximum temperature and the temperature of the grid-cell
Figure 26. P-value of the linear relationship between direct biogeophysical impacts of the conversion from
broadleaf to coniferous forests on monthly mean daily maximum temperature and the temperature of the grid-
cell
Figure 27. Monthly mean temperature differences between simulations with "young" forests: (27-39 years) and
"mature" forests (62-74 years), using the offline land-component JSBACH4
Figure 28. Monthly mean temperature differences between simulations with "old-growth" forests: (>150 years)
and "mature" forests (62-74 years), using the offline land-component JSBACH4

# **List of Tables**

Table 1: Experimental design	10
Table 2: The categorization of grass and forest PFTs for the separation of direct and indirect effects	11



# **Abbreviations**

**COSMO-CLM** Consortium for Small-scale Modelling – Climate Limited-are Modeling Community

**CLM** Community land model

COSMO-CLM<sup>2</sup> Coupled model of COSMO-CLM and CLM

ICON-ESM ICOsahedral Nonhydrostatic Earth System Model

**JSBACH** Jena Scheme for Biosphere-Atmosphere Coupling in Hamburg

**PFT** Plant functional type



# **Executive summary**

This deliverable is a part of the ForestNavigator project Work Package 4 (Biodiversity and ecosystem services) and presents outcomes of task 4.2, which focuses on climate regulation feedbacks associated with forest management. The goal of this task was to develop an emulator (MESMER-L-X) that can quickly and efficiently reproduce biophysical effects resulting from changes in forest management practices.

The work began with model simulations using the regional climate model COSMO-CLM² and model development and exploratory work with the Icosahedral Nonhydrostatic Earth System Model ICON-ESM/JSBACH4 to assess suitable simulation approaches for the project. Due to the higher complexity and adaptation demands of the ICON-ESM simulations in the context of the deliverable, primary efforts were directed towards the COSMO-CLM² simulations. These included several forest land use scenarios, covering afforestation, deforestation, and forest composition changes. The statistical relationship between these forest changes and the near-surface air temperature was investigated and successfully implemented into a novel emulator that can efficiently reproduce the associated effects of these forest changes on the typical local daily mean, maximum, and minimum temperatures.

The emulator can successfully capture the effects seen in the original simulations, such as the spatial patterns of warming associated with afforestation or a conversion to needleleaf trees, the cooling associated with deforestation, or the conversion to broadleaf trees. The equations have been shared with project collaborators, and the emulator's preliminary version is available in a public repository (<a href="https://gitlab.iiasa.ac.at/forestnavigator/wp4/forestnavigator">https://gitlab.iiasa.ac.at/forestnavigator/wp4/forestnavigator</a> d4.3 mesmer-l-x.git).

This emulator will be used to support WP7, where they can be incorporated into the G4M-X metamodel via the modification of climate input parameters. Ultimately, we expect that the emulator may play a valuable role in supporting European forest policymaking by providing fast, reliable insights into the climate impacts of different forest management scenarios.



### I. Introduction

Forests play an important role in European climate policy due to their capacity to absorb and store carbon dioxide. Sustainable forest management, therefore, is a key strategy for achieving the EU's climate neutrality goals (Grassi et al., 2017). As natural carbon sinks, forests can help offset greenhouse gas emissions from other sectors, such as energy and transportation (Whitehead, 2011). They also contribute to biodiversity conservation, soil protection, and water regulation, which are integral to climate adaptation strategies. European policies like the EU Forest Strategy and the Regulation on land use, land-use change and forestry (LULUCF) underscore the importance of sustainable forest management in enhancing carbon sequestration while ensuring the resilience and health of forest ecosystems (Romppanen, 2020). By preserving and restoring forests, Europe can strengthen its efforts to combat climate change and protect environmental sustainability.

Beyond their role in carbon sequestration, forests can also have pronounced biogeophysical impacts that influence climate at both regional and global scales (Winckler et al., 2018; Davin et al., 2020; De Hertog et al., 2022, Pongratz et al., 2021). These effects include changes in albedo, surface roughness, and evapotranspiration efficiency. Forests typically have a lower albedo than open land (such as grasslands), meaning that they absorb more solar radiation, which can lead to localized warming (Kirschbaum et al., 2011). However, this is often counterbalanced by increased evapotranspiration, which cools down the near-surface air through the release of water vapor (Ellison et al., 2024). Additionally, forests influence wind patterns and cloud formation due to their complex structure and surface roughness (Teuling et al., 2017; Belušić et al., 2019).

Given the complexity and significance of these processes, climate and Earth System models can serve as useful tools for projecting climate impacts of different forest systems. However, these models generally consume large amounts of computational resources. This issue can be addressed by developing climate model emulators. They serve as simplified, computationally faster versions of complex climate models, allowing researchers to rapidly explore a wide range of scenarios and variables without the need for resource-intensive simulations (Beusch et al., 2021). Using emulators enables quicker decision-making, especially in policy and planning contexts, where timely insights are essential. Additionally, emulators are particularly valuable for uncertainty analysis, helping to identify key drivers of climate change impacts and assess potential risks across various sectors (Nath et al., 2023). By providing faster feedback on potential climate futures, emulators support informed decision-making for climate adaptation and mitigation strategies, facilitating more effective and responsive climate action.

In this report, we describe the development of an emulator capable of reproducing direct biogeophysical impacts of forest changes across Europe, using a set of simulations conducted with the COSMO-CLM² model, a regional climate model that is coupled with a land model. We outline the process of creating the emulator, named MESMER-L-X, starting from solving the challenge of extracting local effects from the simulations. Once local effects could be extracted, the next step consisted of comparing COSMO-CLM² climate simulations with modified forestation strategy against control simulations that have a current land-use distribution. The forest changes considered include variations in forest cover (afforestation, deforestation), shifts in forest composition (i.e., changes in the fractions of coniferous and broadleaf forests), as well as their combined effects. From there, statistical relationships between local temperature effects associated with each land-use change were identified through analysis of monthly means of daily mean, minimum, and maximum temperatures. As the last step, the emulator was then constructed based on these identified statistical relationships. The final MESMER-L-X emulator operates by



taking temperature data as input and applying the land-use change effects to generate the resulting modified temperature variables as output.

The initial ForestNavigator project proposal also envisioned the integration of the Earth system model ICON-ESM simulations into the development of MESMER-L-X. In this context, ICON-ESM more specifically refers to ICON-ESM coupled with JSBACH4, as JSBACH4 has a more detailed forest growth representation. The original aim of using the two models was to increase confidence in the results through two independent sets of simulations. However, due to delays and modeling limitations (late hiring/change in staff due to challenging applicant situation for both institutions, slower than anticipated community progress on ICON-ESM features anticipated to be available by the time of the WP start, higher than anticipated complexity in integrating G4M-X forestry information into ICON-ESM and COSMO-CLM²), different strategies were adopted: rather than using the two models for robustness, the focus diverged toward developing specific emulators capturing different processes (forest cover and composition changes for COSMO-CLM², forestry/age-dependent climate effects for ICON-ESM), and an initial focus of the joint effort on the COSMO-CLM²-based emulator to ensure its timely delivery to the other ForestNavigator partners.

# 2. Forest scenarios simulated with COSMO-CLM<sup>2</sup>

## 2.1. Simulation setup

In this study, the Consortium for Small-scale Modelling - Climate Limited-area Modeling Community (COSMO-CLM) regional climate model, coupled with the Community Land Model (CLM), was employed to simulate regional climate processes with high spatial and temporal resolution (0.44°x0.44° for the atmosphere and 0.5°x0.5° for the land model (~50 km), 30 minutes time step). This coupled modeling system, hereafter referred to as COSMO-CLM² ("COSMO-CLM squared") (Davin et al., 2011), allows for a more comprehensive representation of land-atmosphere interactions by integrating the detailed surface processes simulated by CLM (version 5) with the atmospheric dynamics of COSMO-CLM. The use of COSMO-CLM² enabled improved simulation of key regional climate features, such as temperature, precipitation, and surface energy fluxes, which are critical for accurately assessing the impacts of climate variability and change at the regional scale.

To better represent the heterogeneity within one grid cell, a sub-gridcell structure was designed by organizing each grid cell into multiple hierarchical levels: land units, columns, and plant functional types (PFTs). Land units represent broad surface types within gridcells such as vegetated land, urban areas, lakes, glaciers, and wetlands (Lawrence et al., 2019; Figure 1). Within each land unit, the model defines columns to account for variations in soil and hydrological processes, such as differences between irrigated and non-irrigated areas. Finally, within each column, the surface patch is further divided into PFTs, which represent specific vegetation types. This layered structure allows CLM5 to simulate the distinct biogeophysical and biogeochemical processes associated with each land type and vegetation class, improving the model's ability to represent complex land-atmosphere interactions at sub-grid scales.



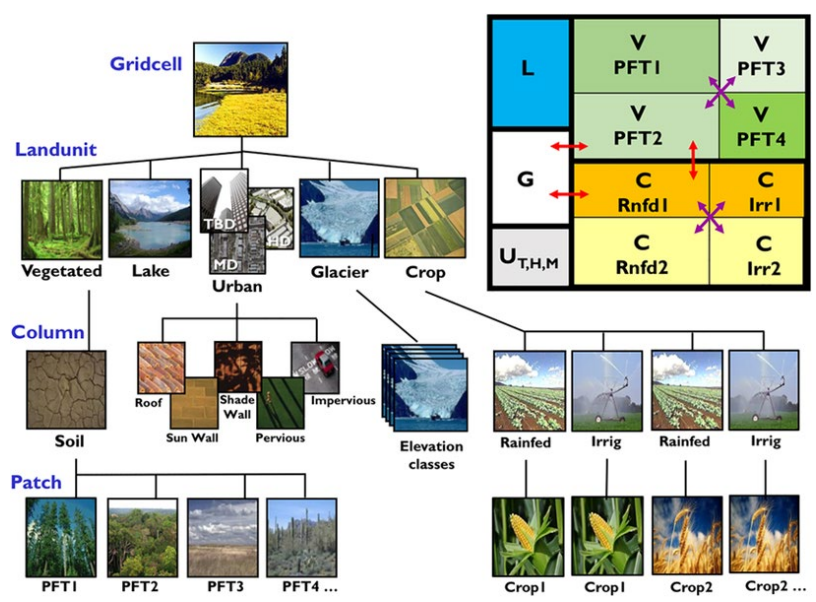


Figure 1. Sub-grid cell level structure of the Community Land Model version 5 (CLM5; from Lawrence et al., 2019). Land units are indicated in the top right panel: L = lake, G = glacier, U = urban, V= natural vegetation and cropland. The arrows indicate how transitions in land-use change can occur in the model.

Seven experiments were conducted using data covering the period 2015 to 2074, with the first 10 years as the spin-up period. The only difference among these seven experiments is the land-use input, which remains static during the whole simulation period (Table 1). The boundary condition input data is from the output of MPI-ESM under the framework of CMIP6 under the scenario SSP3-7.0, and the reason why we chose this scenario is that it can induce the highest warming level (Wieners et al., 2019). The control experiment (Ctl) represents present-day land-use conditions and serves as the reference for comparison. The Afforestation scenario (Aff) simulates the conversion of all grasslands to forests, maintaining the existing forest composition. Conversely, the Deforestation scenario (Def) involves converting all forests into grassland. Two experiments focus on forest composition changes: Brd replaces all coniferous forests with broadleaf forests, while Ndl does the opposite by replacing all broadleaf forests with coniferous forests. The AfB scenario combines afforestation with compositional change by converting both grassland and coniferous forests to broadleaf forests. Similarly, the AfN experiment replaces all grassland and broadleaf forests with coniferous forests. Together, these experiments enabled a detailed analysis of how different aspects of forest cover and composition influence land-atmosphere interactions and regional climate.

Table 1: Experimental design

Experiment	Land-use input
Ctl	Present-day land-use
Aff	Replacing all grassland with forests, without changing the forest composition
Def	Replacing all forests with grassland
Brd	Replacing all coniferous forests with broadleaf forests
Ndl	Replacing all broadleaf forests with coniferous forests
AfB	Replacing all grassland and coniferous forests with broadleaf forests
AfN	Replacing all grassland and broadleaf forests with coniferous forests

The goal for the emulator is to capture direct impacts – effects in the location where the changes occur and are directly caused by the forest land-use changes in this location. Therefore, direct impacts need to be separated from indirect impacts, and we utilized the sub-grid level outputs of



CLM5 to do this. Relevant to the experiments (Table 1), changes occur over the forest and grass PFTs (Figure 1). Within the natural vegetation land-unit and column of COSMO-CLM<sup>2</sup>, there are 3 coniferous tree species, five broadleaf tree species, and 3 grass species, which for this purpose are grouped together in these main functional categories (Table 2). Shrubland and bare ground are categorized into a land use tile called "other", together with other land-use units like cropland, lakes, urban areas, and glaciers.

Table 2: The categorization of grass and forest PFTs for the separation of direct and indirect effects.

Plant Functional Type	Category
Bare Ground	Other
Needleleaf evergreen tree – temperate	Coniferous forests
Needleleaf evergreen tree - boreal	Coniferous forests
Needleleaf deciduous tree – boreal	Coniferous forests
Broadleaf evergreen tree – tropical	Broadleaf forests
Broadleaf evergreen tree – temperate	Broadleaf forests
Broadleaf deciduous tree – tropical	Broadleaf forests
Broadleaf deciduous tree – temperate	Broadleaf forests
Broadleaf deciduous tree – boreal	Broadleaf forests
C3 arctic grass	Grassland
C3 grass	Grassland
C4 grass	Grassland

We explain this process of separating direct and indirect effects using the experiment Aff as an example, which is visualized in Figure 2. Assuming that we have a grid cell, which in the control simulation is divided into three land-use tiles: forest (green: F), grassland (light green: G), and other (orange: O). In the afforestation simulation, grasslands are converted into forest, so there are only two land-use types left.



Figure 2. Visual example of the separation process of direct and indirect impacts

We define temperatures before afforestation over each land-use type as  $T_f$ ,  $T_g$ , and  $T_o$ , and the temperatures after afforestation over each land-use type are  $T_f'$  and  $T_o'$ . A basic assumption is that the indirect impacts ( $\Delta T_{ind}$ ) are the same over the whole grid cell, which can be calculated as

$$\Delta T_{ind} = \left( (T'_o - T_o) \times F_o + \left( T'_f - T_f \right) \times F_f \right) \div \left( F_f + F_o \right)$$

, where  $F_f$  and  $F_o$  indicate the fraction of forest and other land-use tiles in the grid cell before afforestation. Consequently, the direct impacts  $\Delta T_{dir}$  can be calculated as:

$$\Delta T_{dir} = T_f' - T_g - \Delta T_{ind}$$

A corresponding method is used for the separation of impacts induced by other forest changes.



### 2.2. Modelled biophysical responses

In this section, we present the results from the above-described experiments regarding forest-changes-induced impacts on temperature. The Forest changes included afforestation, deforestation, forest composition change, etc. (Table 2). For each month, the results of the monthly mean daily maximum temperature changes are analyzed here, and the results of daily mean and daily minimum temperature are also calculated (not presented in this report). Both direct and indirect impacts are presented here for comparison. All results shown below are the difference between the corresponding experiment and the control simulation. In this section, we only present the results of four experiments, Aff, Def, Brd, and Ndl in this section. The results from AfB and AfN are approximately the sum of Aff and Brd or Ndl, which are provided in the netCDF files prepared for emulator users.

### 2.2.1. Afforestation

Afforestation (grassland to forests) induces pronounced biogeophysical impacts on 2-meter air temperature across Europe, with distinct spatial and seasonal patterns for both direct and indirect effects. The direct effects result in widespread warming throughout the year, especially during the spring and summer months (Figure 3). Notably, from April to July, northern and eastern Europe experience direct temperature increases exceeding +1.2°C compared to the control simulation average over the period 2025-2074, and similar warming is also observed in many grid cells over southern regions.

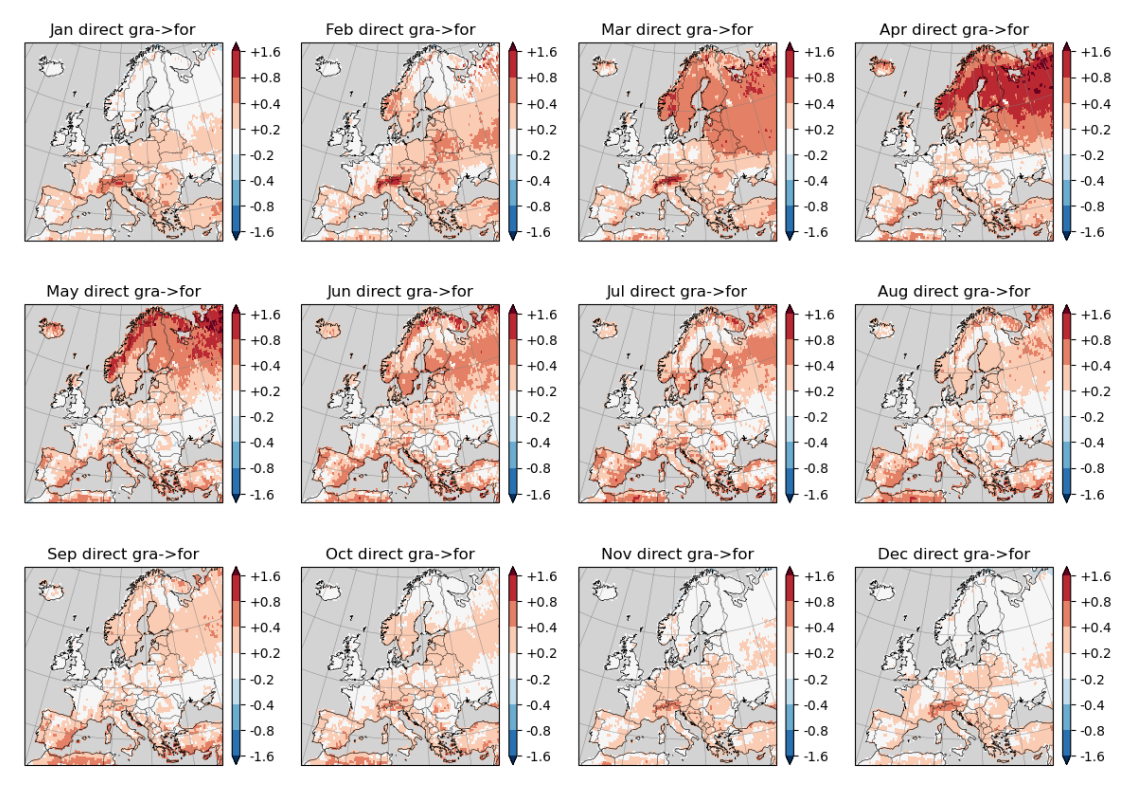


Figure 3. Direct biogeophysical impacts of the conversion from grassland to forests on average (2025-2074) monthly mean daily maximum temperature (in K)

In contrast, the indirect effects show a more heterogeneous response (Figure 4), which is likely mediated by changes in soil moisture and evapotranspiration. Indirect warming is dominant in the boreal and temperate zones, particularly from March to May, with northern Europe consistently



experiencing warming effects exceeding +1.0°C relative to the control simulation. During summer (July–August), indirect warming effects disappear in the Northern regions but occur in parts of southern and eastern Europe, potentially due to moisture-related feedbacks.

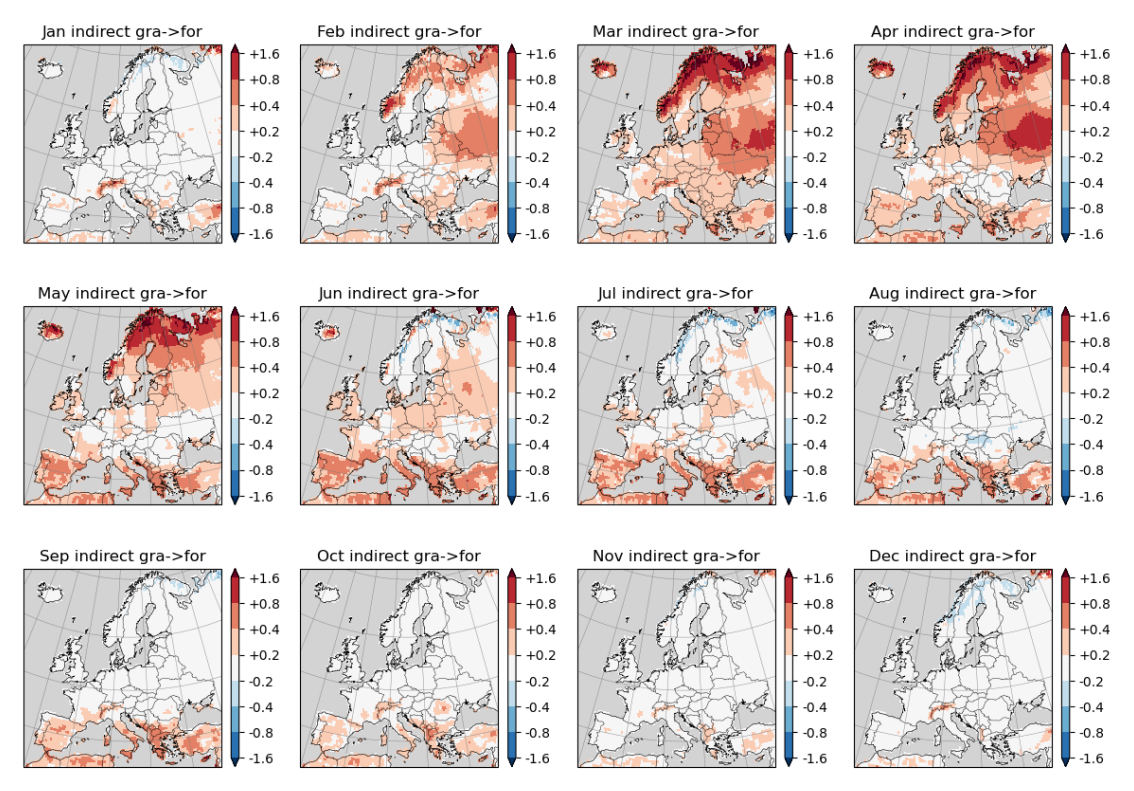


Figure 4. Indirect biogeophysical impacts of the conversion from grassland to forests on average (2025-2074) monthly mean daily maximum temperature (in K)

#### 2.2.2. Deforestation

Direct effects of deforestation (forests to grassland, Figure 5) predominantly indicate a cooling signal throughout most of the year, particularly over southern and eastern Europe, with the strongest cooling (>0.8 or even 1.6 °C in many grid cells) observed during the spring and summer months. Some localized warming appears in northern latitudes, especially in winter.

In contrast, the indirect effects (Figure 6) are more spatially extensive and show stronger cooling across northern and eastern Europe from February to July, peaking in spring and early summer (over 1.6 °C). Interestingly, indirect warming emerges in the boreal regions during late autumn and early winter, suggesting a seasonal shift in feedback such as changes in cloud cover or surface albedo.



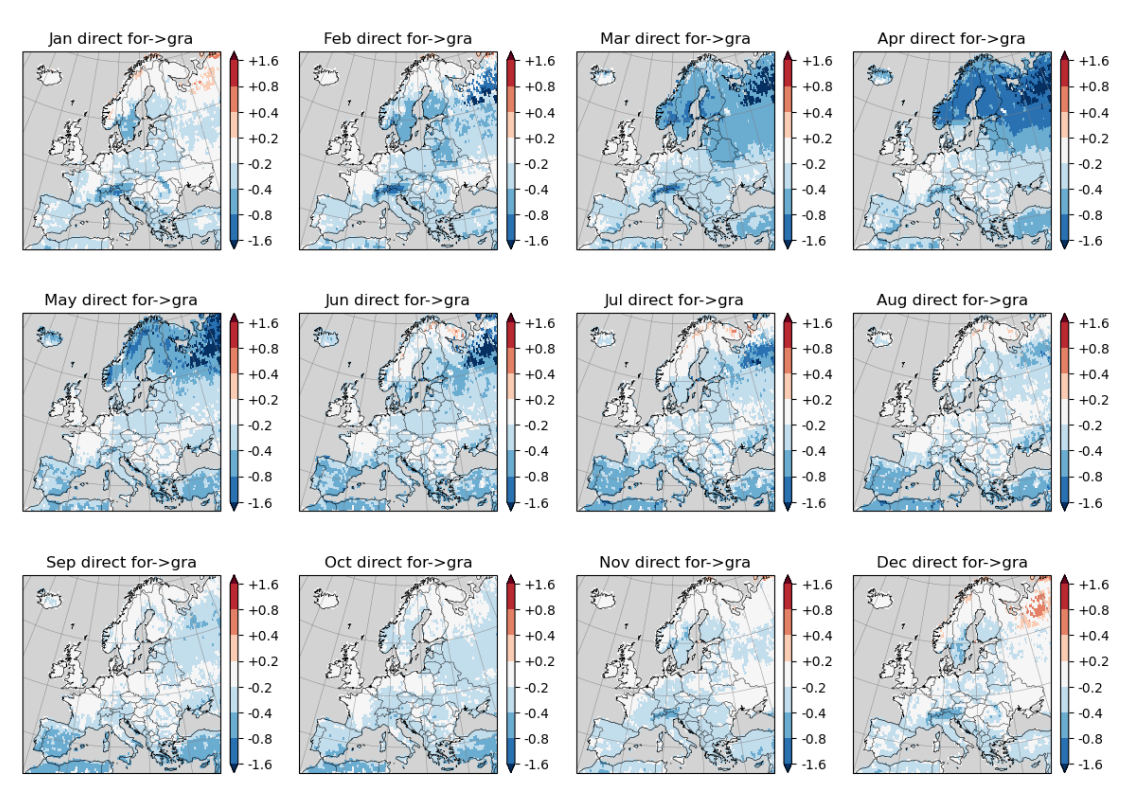


Figure 5. Direct biogeophysical impacts of the conversion from forests to grassland on average (2025-2074) monthly mean daily maximum temperature (in K)

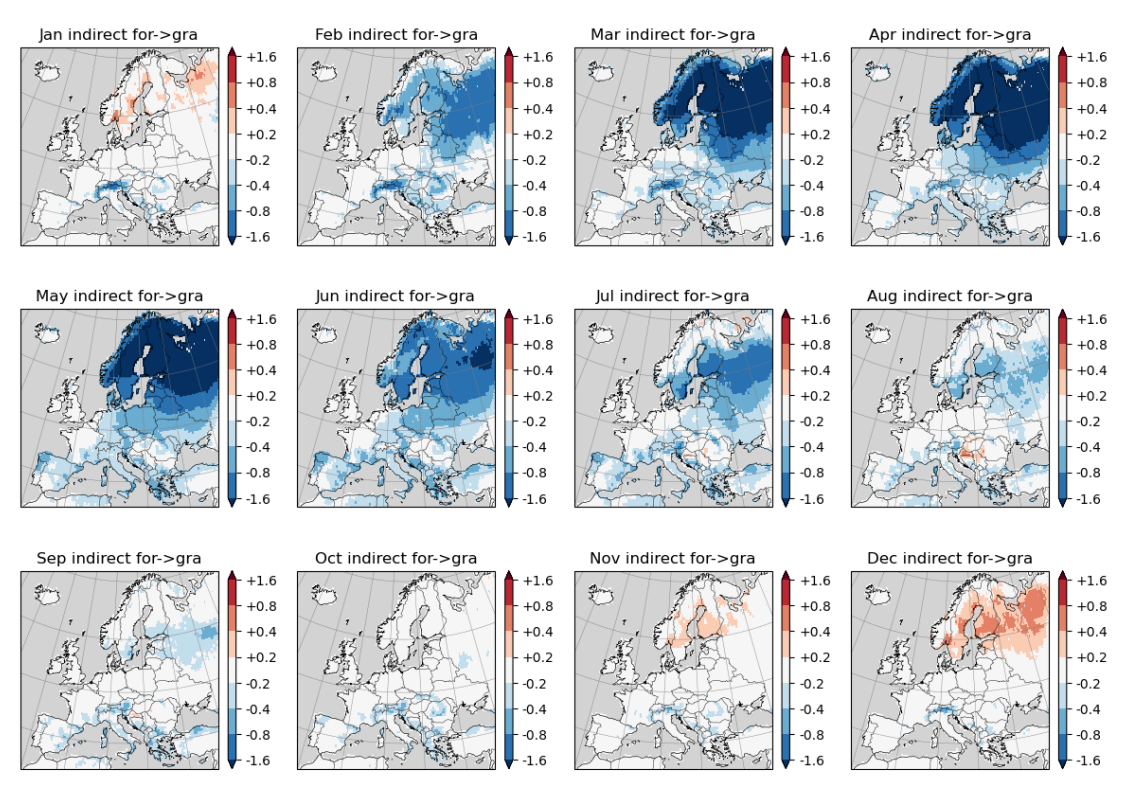


Figure 6. Indirect biogeophysical impacts of the conversion from forests to grassland on average (2025-2074) monthly mean daily maximum temperature (in K)

#### 2.2.3. Conversion from needleleaf to broadleaf

The seasonal patterns of biogeophysical effects resulting from the conversion of needleleaf (coniferous) to broadleaf forests reveal nuanced temperature responses across Europe (Figure 7).



The direct effects indicate a slight tendency toward cooling across most of the continent, with enhanced responses in Scandinavia and parts of Eastern Europe from April through July (more than 0.4 °C in many grid cells).

In contrast, the indirect effects (Figure 8) show a stronger response and a marked cooling signal during spring and summer months, especially across northern and eastern Europe, with temperature reductions reaching up to  $-1.6^{\circ}$ C in some regions. This cooling is most prominent from March to August, suggesting a strong influence of changes in surface albedo, evapotranspiration, and atmospheric feedbacks during the growing season. Conversely, weak warming appears in northern latitudes during winter months, particularly in December and January.

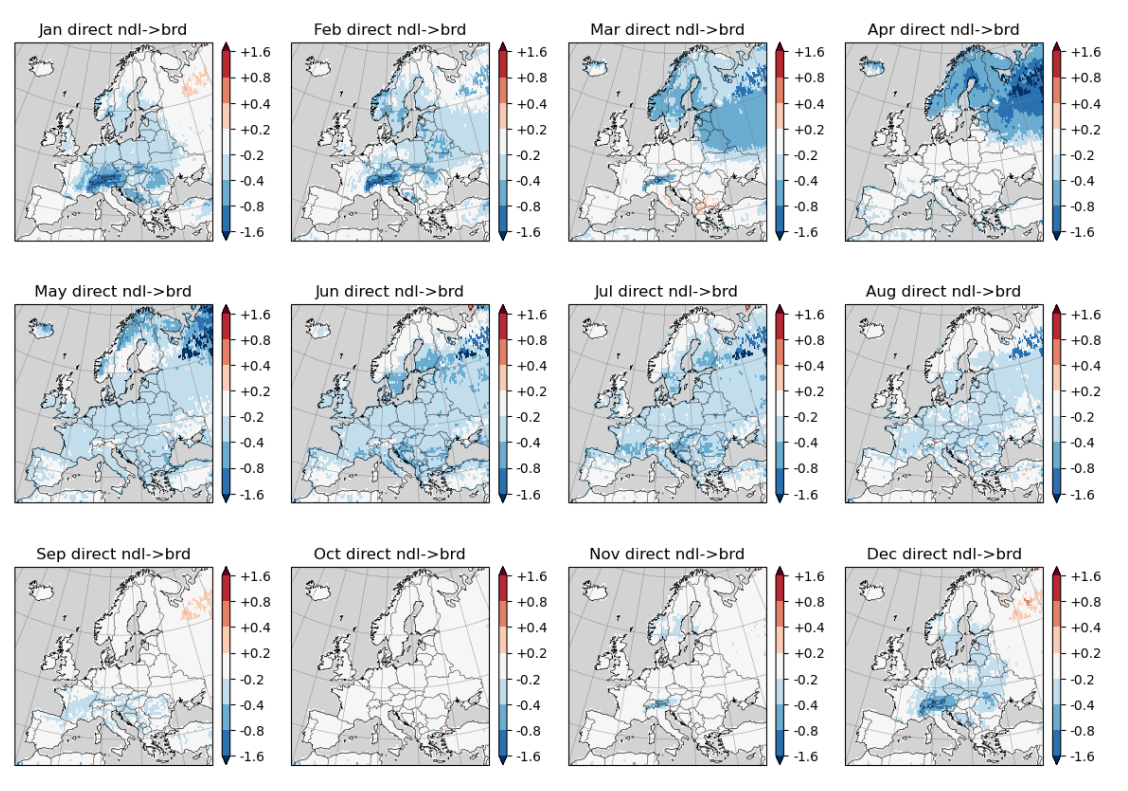


Figure 7. Direct biogeophysical impacts of the conversion from coniferous forests to broadleaf forests on average (2025-2074) monthly mean daily maximum temperature (in K)



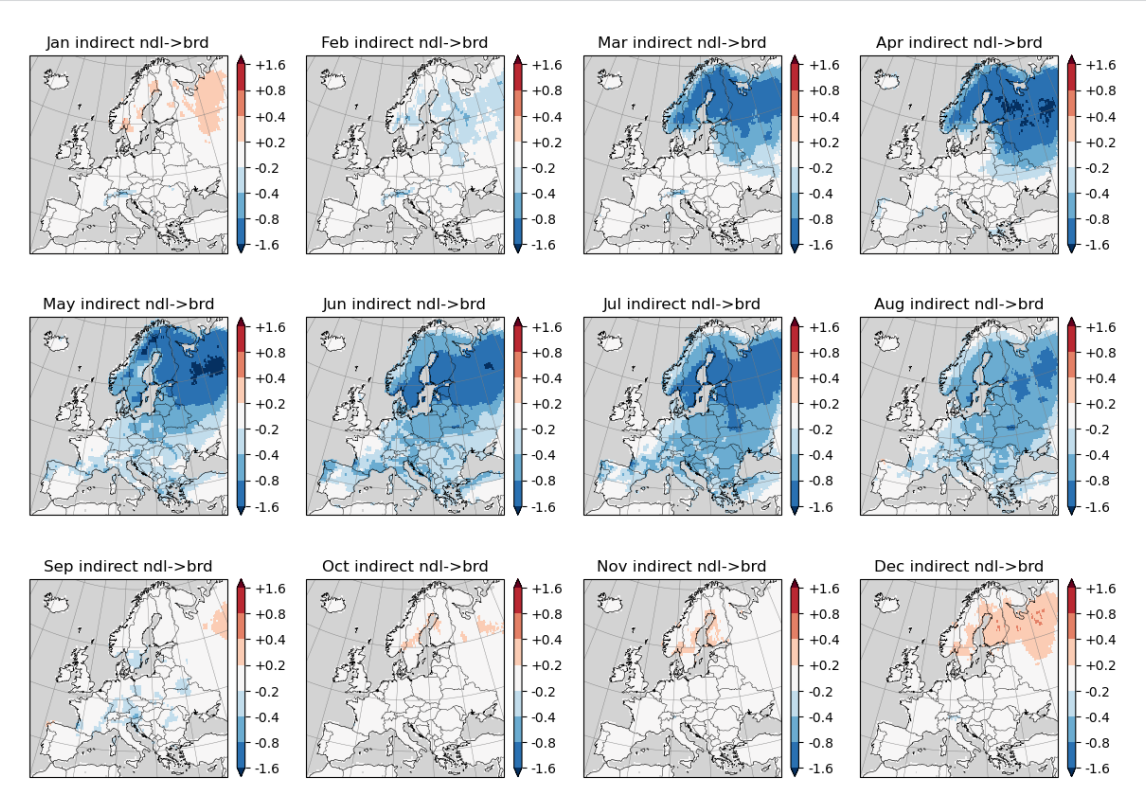


Figure 8. Indirect biogeophysical impacts of the conversion from coniferous forests to broadleaf forests on average (2025-2074) monthly mean daily maximum temperature (in K)

### 2.2.4. Conversion from broadleaf to needleleaf

The conversion from broadleaf to needleleaf forests yields a predominantly warming biogeophysical signal across Europe, as indicated by both direct and indirect effects on 2-meter daily maximum temperature. The direct effects (Figure 9) reveal widespread warming throughout the year, with the most substantial increases in temperature occurring over northern and eastern Europe during spring and summer (March–August), where anomalies often exceed +0.8°C. This warming is likely linked to the lower albedo and greater canopy roughness of needleleaf forests.

The indirect effects (Figure 10) reinforce this pattern, showing an even stronger and more spatially extensive warming response from late spring through summer, particularly over southeastern and eastern Europe, with July and August seeing peak warming of up to +1.6°C in some areas.



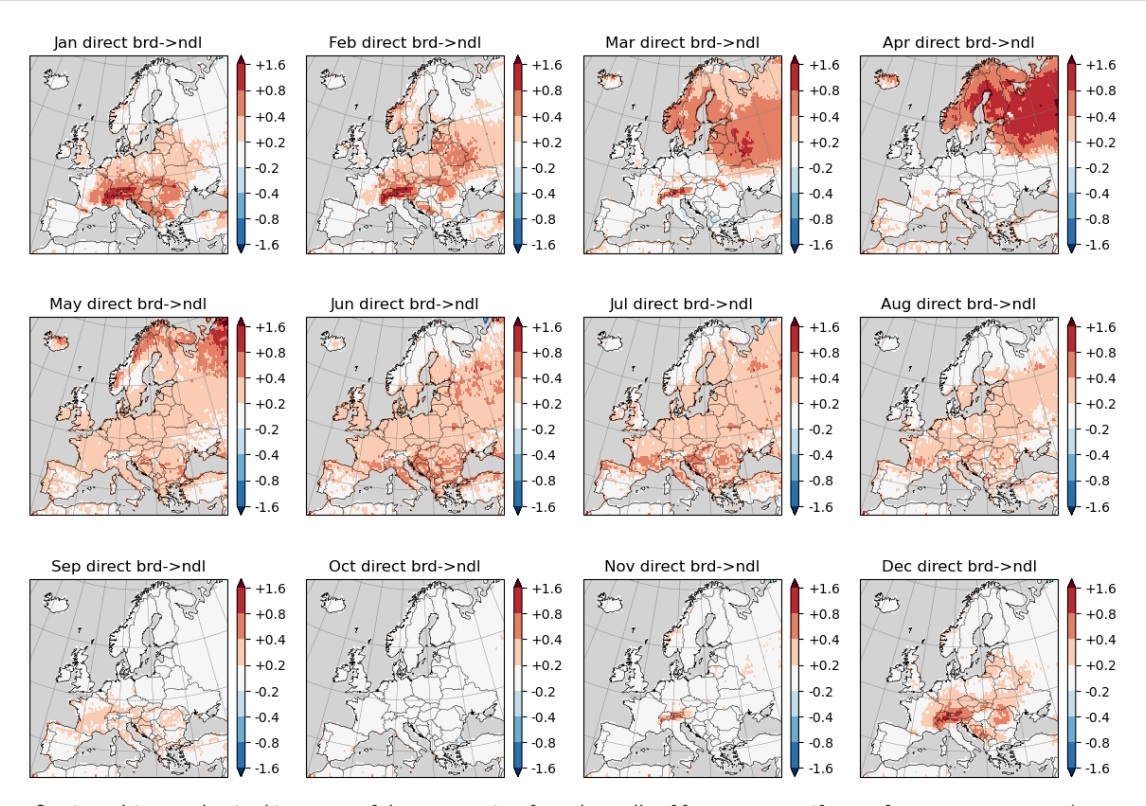


Figure 9. Direct biogeophysical impacts of the conversion from broadleaf forests to coniferous forests on average (2025-2074) monthly mean daily maximum temperature (in K)

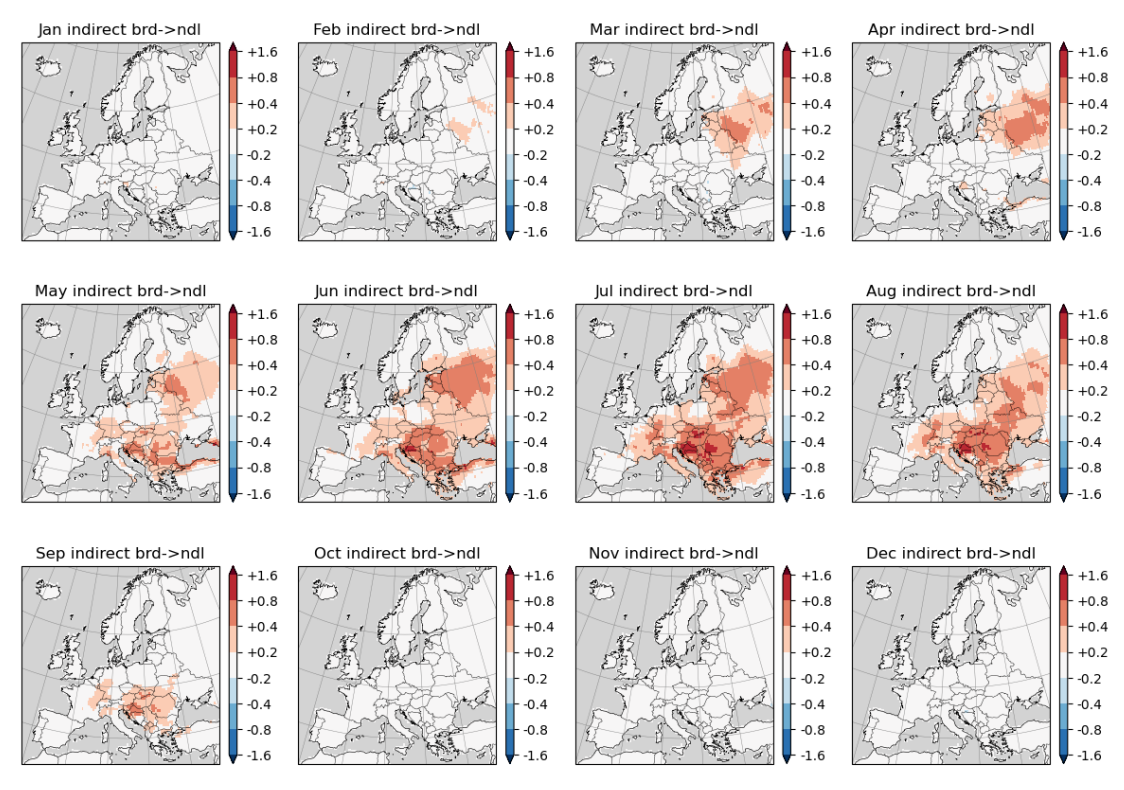


Figure 10. Indirect biogeophysical impacts of the conversion from broadleaf forests to coniferous forests on average (2025-2074) monthly mean daily maximum temperature (in K)



# 3. Development of the MESMER-L-X Emulator

### 3.1. Formulation of the emulator equations

MESMER-L-X is designed to emulate the direct impacts of forest changes on near-surface temperature. This is a new emulator dedicated to reproducing the direct biogeophysical impacts of forest change, while previous MESMERs focus on reproducing the spatial distribution of mean or extreme temperatures from a global mean temperature (Beusch et al., 2020; Nath et al., 2021; Quilcaille et al., 2023). As outlined above, direct impacts indicate the impacts directly induced by forest change, which only occur over the land-use tile where forests change. Indirect impacts are the impacts caused by advection and general circulation.

Like previous MESMER emulators, the emulator designed in this study could be divided into two parts: a local response module and a local residual variability module. The local response module is based on the relationship between the direct impacts of forest change and local grid cell temperature, while the local residual variability module is used for reproducing the local variability.

The linear relationship between the direct impacts of forest change and local grid cell temperature is built based on the simulations from the years 2015-2074 (60 values for each month). Thus, it can be represented as:

$$T_{s,t,m}^{resp} = \beta^{trend} \cdot T_{s,t,m} + \beta^{int}$$

Where  $T_{s,t,m}^{resp}$  is the response temperature change calculated based on the linear relationship,  $\beta^{trend}$  indicates the slope and  $\beta^{int}$  indicates the intercept. The local residual variability should roughly follow a Gaussian distribution:

$$\eta(0,\sigma)$$

, where  $\sigma$  indicates the standard deviation. Thus, the whole emulated temperature should be

$$T_{s,t,m}^{emu} = \beta^{trend} \cdot T_{s,t,m} + \beta^{int} T_{s,t,m} + \eta(0,\sigma)$$

Where  $T_{s,t,m}^{emu}$  is the emulated temperature change. The slope and intercept of the linear relationship are different for different types of forest change scenarios, and also different for monthly mean, daily mean, daily maximum, and daily minimum temperatures.

To conclude, there are three parameters:  $\beta^{trend}$ ,  $\beta^{int}$ , and  $\sigma$ , which need to be calculated through the training based on COSMO-CLM2 simulations, in which the slope ( $\beta^{trend}$ ) represents the sensitivity of direct temperature change to the background temperature, and the standard deviation ( $\sigma$ ) indicates the uncertainty level of the linear relationship. Moreover, we also use two indices, R-squared value and p-value, to evaluate the robustness of the linear relationship we build.

# 3.2. Statistical relationships between forest type changes and temperature variables

### 3.2.1. Afforestation

Positive slopes dominate during summer months (May–August), especially across central and northern Europe, suggesting that forest changes tend to amplify warming during already warm months (Figure 11). Conversely, in spring (March–April) and autumn (September–October), negative slopes appear in parts of Scandinavia, indicating a dampening response. The residual



standard deviation plots (Figure 12) show where the uncertainty in the linear relationship is highest. Peak residual variability occurs in northern and eastern Europe from March to August, reflecting greater local temperature variability not explained by the linear model. The R-squared maps (Figure 13)—measuring the proportion of variance explained—reveal relatively strong model performance during summer months, especially in Scandinavia and central Europe, where values exceed 0.5 in many grid cells. In contrast, lower R-squared values are seen in western and southern Europe during winter, indicating that the linear relationship is weaker or more influenced by residual variability during those periods. Finally, the p-value maps (Figure 14) confirm that most slope coefficients are statistically significant (p < 0.05) over large parts of the continent, particularly from April through September.

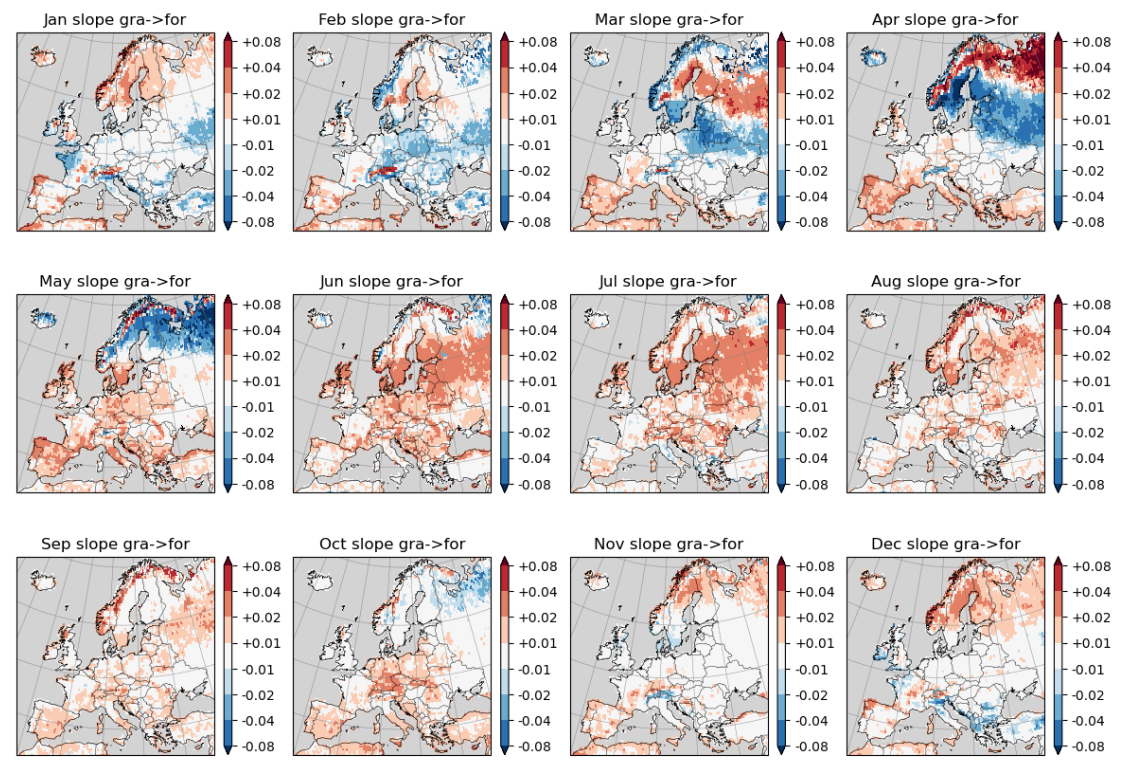


Figure 11. Slope of the linear relationship between direct biogeophysical impacts of the conversion from grassland to forests on monthly mean daily maximum temperature and the temperature of the grid-cell



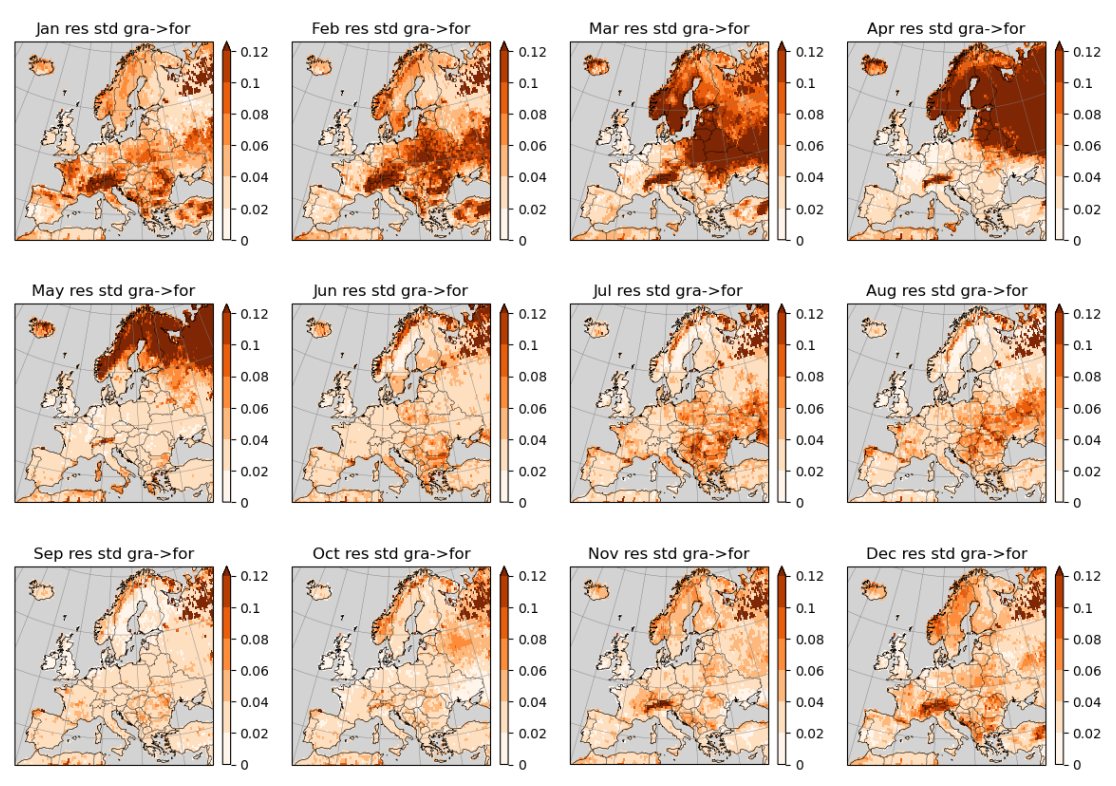


Figure 12. Standard deviation of the residual calculated based on the linear relationship between direct biogeophysical impacts of the conversion from grassland to forests on monthly mean daily maximum temperature and the temperature of the grid-cell

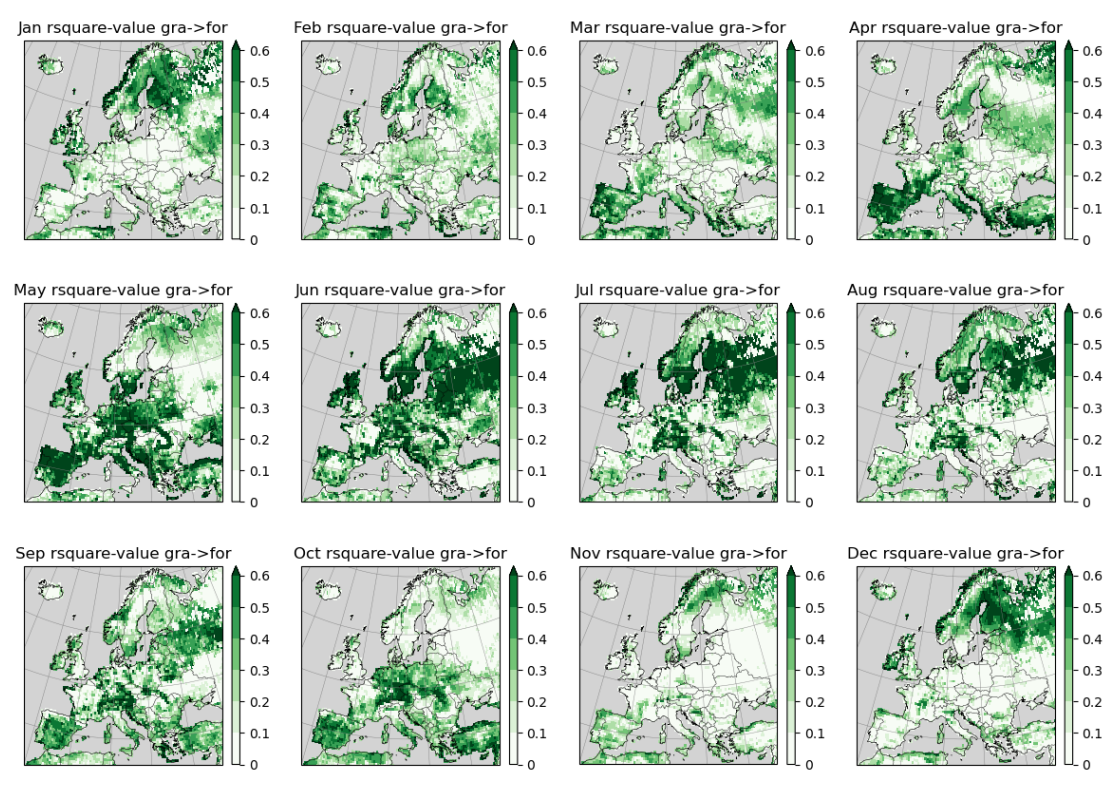


Figure 13. R-square value of the linear relationship between direct biogeophysical impacts of the conversion from grassland to forests on monthly mean daily maximum temperature and the temperature of the grid-cell



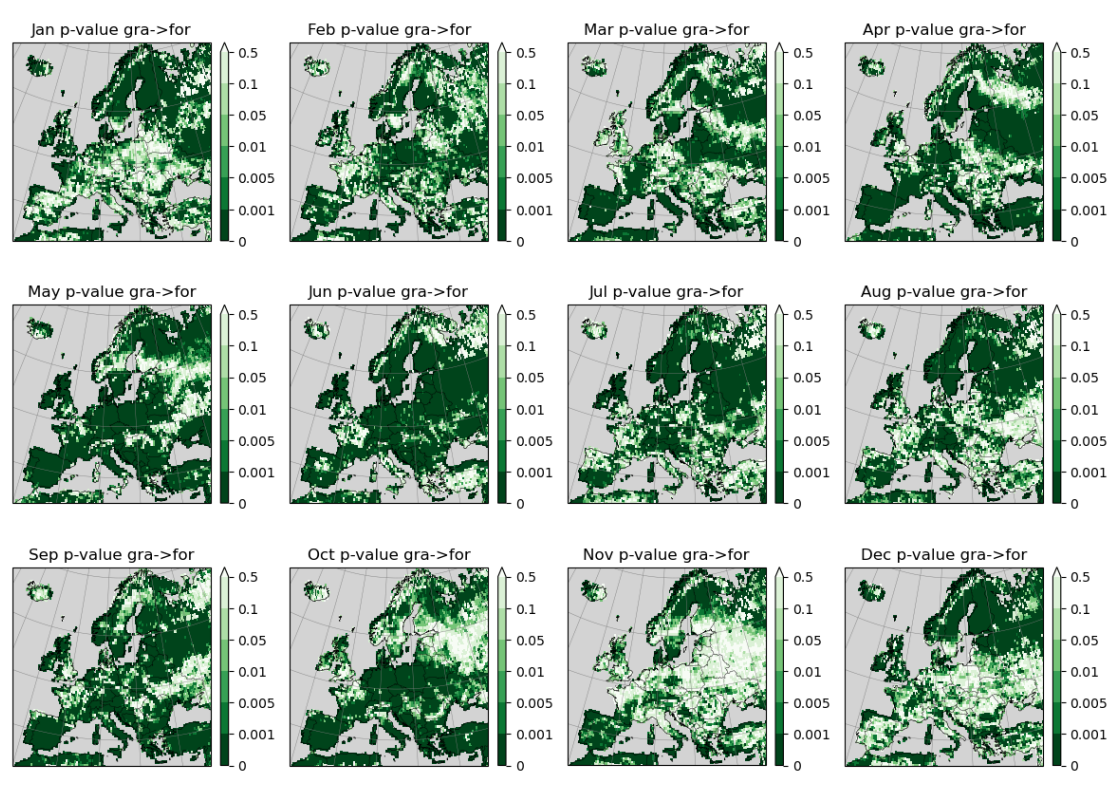


Figure 14. P-value of the linear relationship between direct biogeophysical impacts of the conversion from grassland to forests on monthly mean daily maximum temperature and the temperature of the grid-cell

#### 3.2.2. Deforestation

The slope coefficients (Figure 15) are predominantly negative from June to September across central and southern Europe, indicating a cooling response. In contrast, positive slopes in northern Europe from March to May and again in late autumn (October–December) suggest localized warming responses in colder seasons. Residual standard deviation maps (Figure 16) highlight higher model uncertainty over northern Europe in spring and summer, particularly from April to August. Lower residuals are generally found in western and southern Europe. R-squared values (Figure 17) reveal the model's explanatory power, with particularly high values (up to ~0.6) over Scandinavia, eastern Europe, and parts of central Europe during summer months. P-value maps confirm that the slope parameters are statistically significant (p < 0.05) across large regions during key transition months, notably from April to August (Figure 18). These results suggest that the linear emulator reliably captures deforestation-induced temperature responses in these areas and seasons. However, explanatory power is lower during the winter months and over western Europe, indicating greater influence of residual variability or non-linear processes not captured by the emulator.



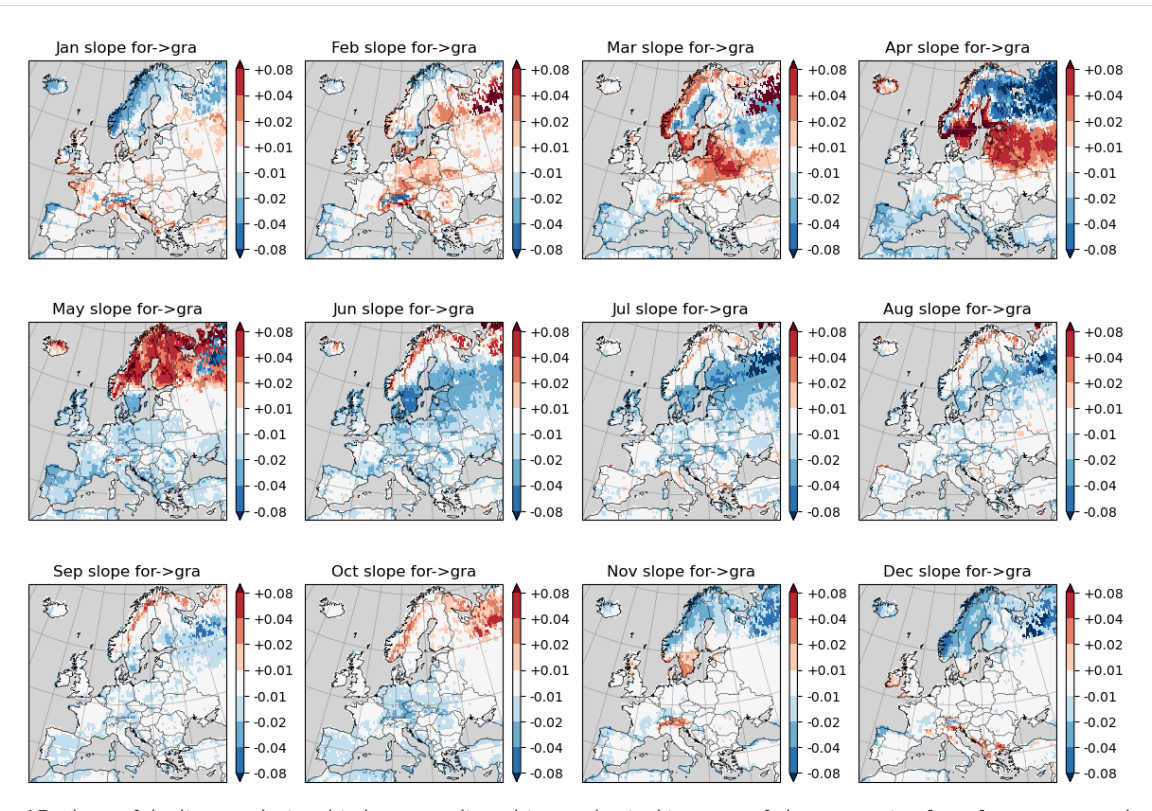


Figure 15. Slope of the linear relationship between direct biogeophysical impacts of the conversion from forests to grassland on monthly mean daily maximum temperature and the temperature of the grid-cell

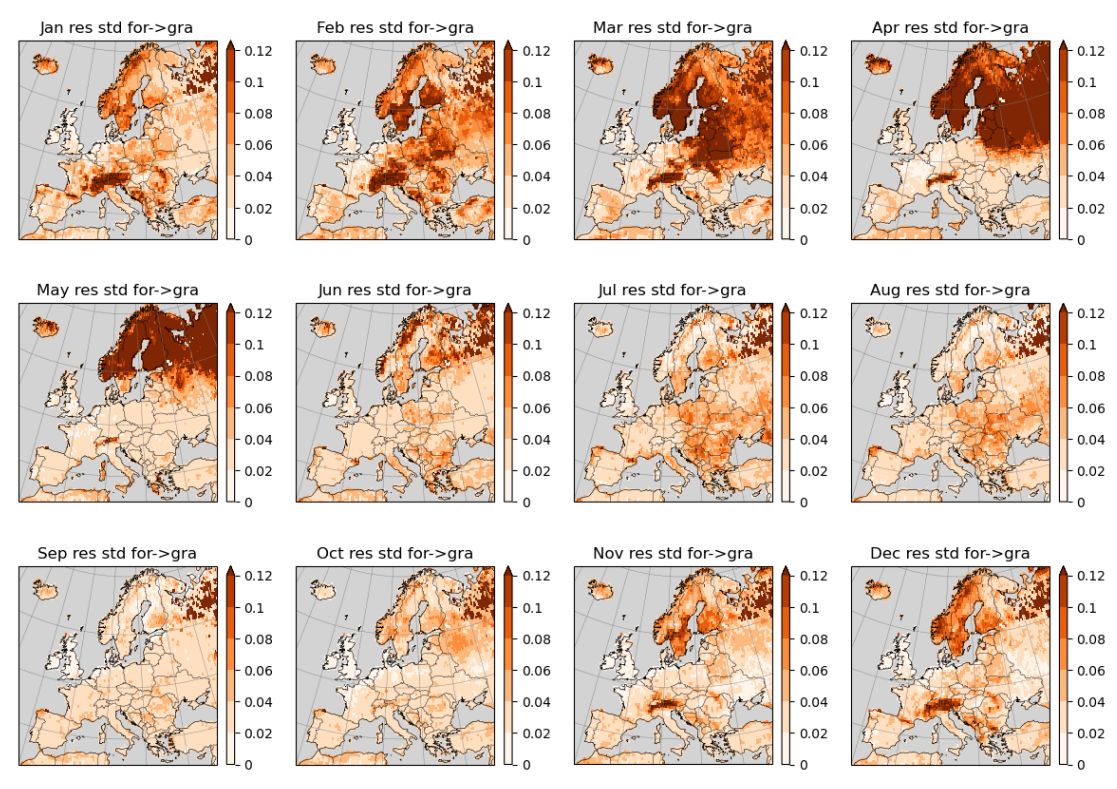


Figure 16. Standard deviation of the residual calculated based on the linear relationship between direct biogeophysical impacts of the conversion from forests to grassland on monthly mean daily maximum temperature and the temperature of the grid cell



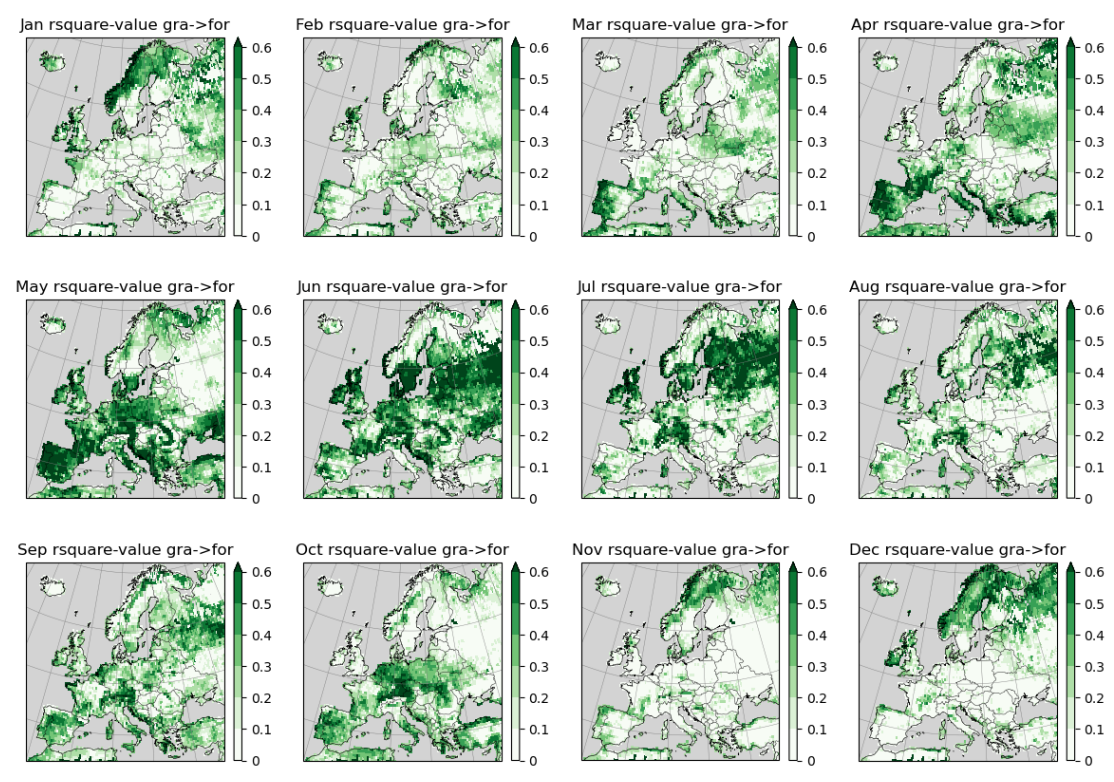


Figure 17. R-square value of the linear relationship between direct biogeophysical impacts of the conversion from forests to grassland on monthly mean daily maximum temperature and the temperature of the grid-cell

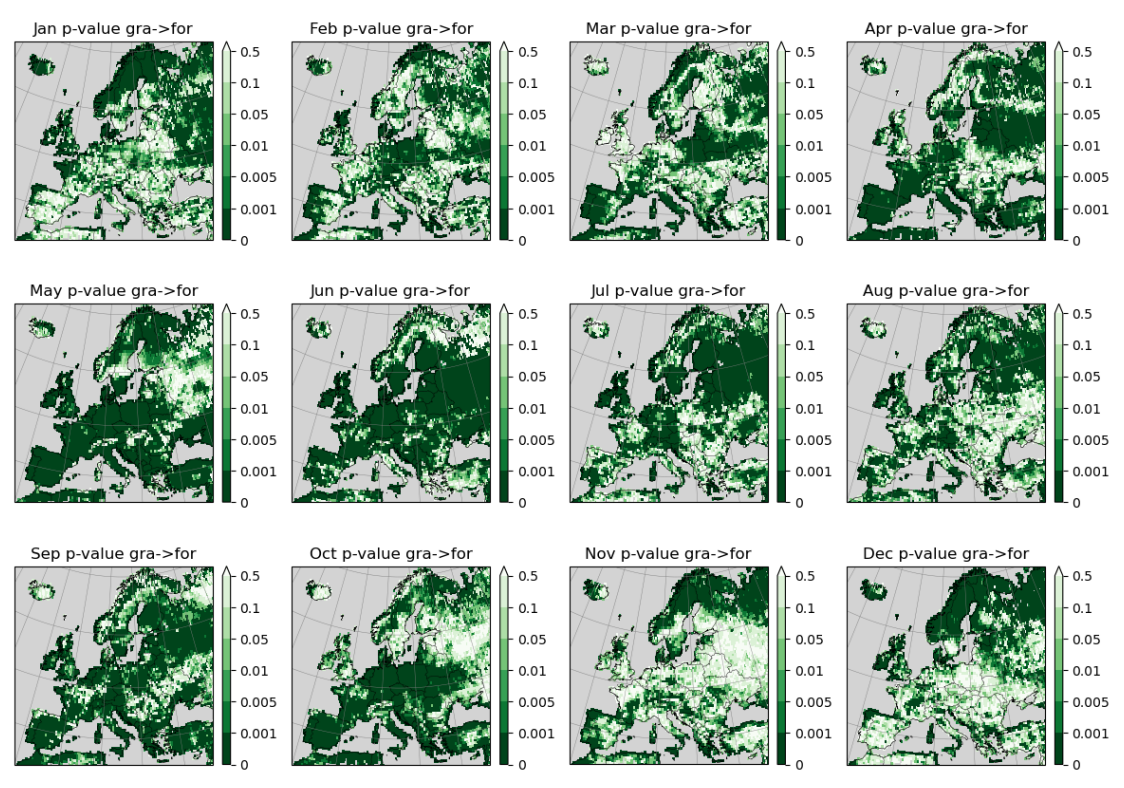


Figure 18. P-value of the linear relationship between direct biogeophysical impacts of the conversion from forests to grassland on monthly mean daily maximum temperature and the temperature of the grid-cell



#### 3.2.3. Conversion to broadleaf forests

The slope coefficients (Figure 19) suggest a distinct pattern: from April to August, northern and northeastern Europe exhibit negative slopes, indicating that the temperature sensitivity to forest-type change is reduced when shifting from coniferous to broadleaf species—consistent with broadleaf forests generally exerting more cooling through enhanced evapotranspiration and higher albedo. Model residual variability, as indicated by the standard deviation maps (Figure 20), is highest during the spring and early summer in boreal and eastern European regions—periods with greater land-atmosphere coupling and phenological transitions, which are harder to capture with simple linear models. The R-squared values (Figure 21) illustrate strong model performance in northern and eastern Europe during summer (up to  $\sim$ 0.6), aligning with the regions and periods where temperature responses to forest type change are most pronounced. Conversely, lower explanatory power is observed in winter and over western Europe, suggesting greater influence from local residuals or nonlinear processes not fully captured in the emulator structure. P-value maps confirm the statistical robustness of the slope coefficients across most of Europe during key growing season months, with widespread significance (p < 0.05) in April–August, especially in high-latitude and continental interiors (Figure 22).

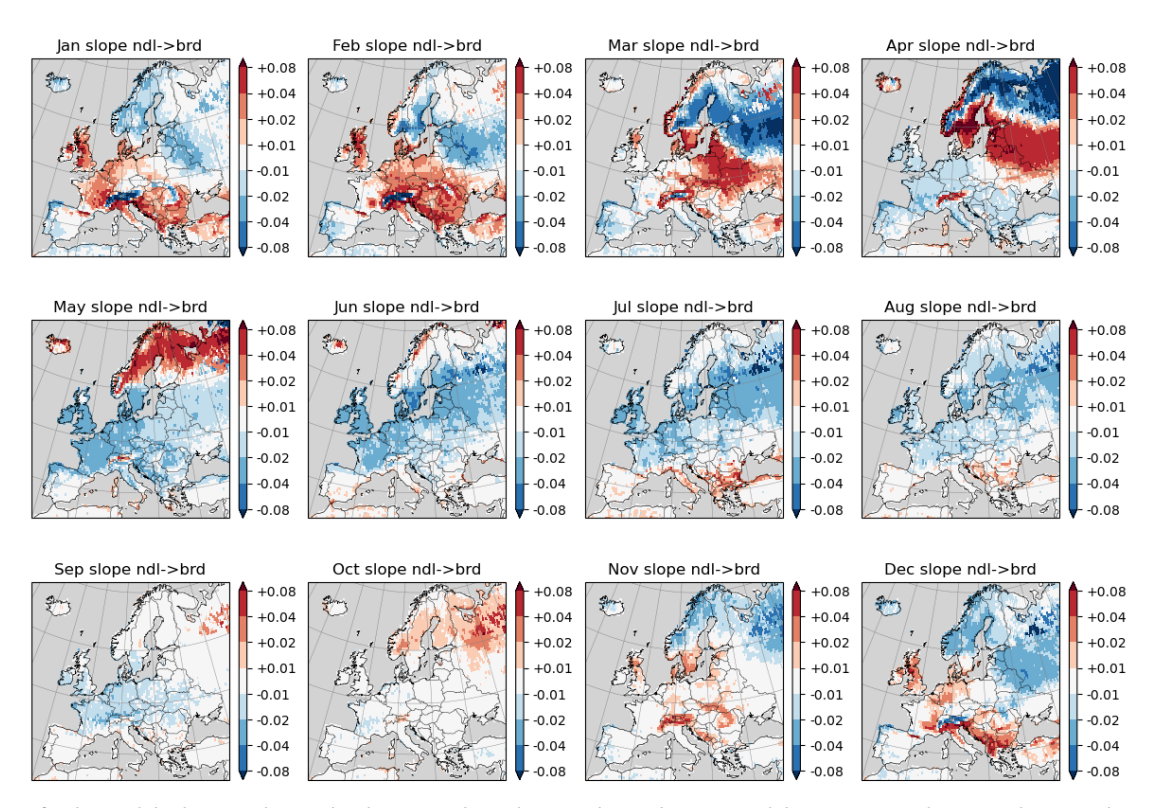


Figure 19. Slope of the linear relationship between direct biogeophysical impacts of the conversion from coniferous to broadleaf forests on monthly mean daily maximum temperature and the temperature of the grid-cell



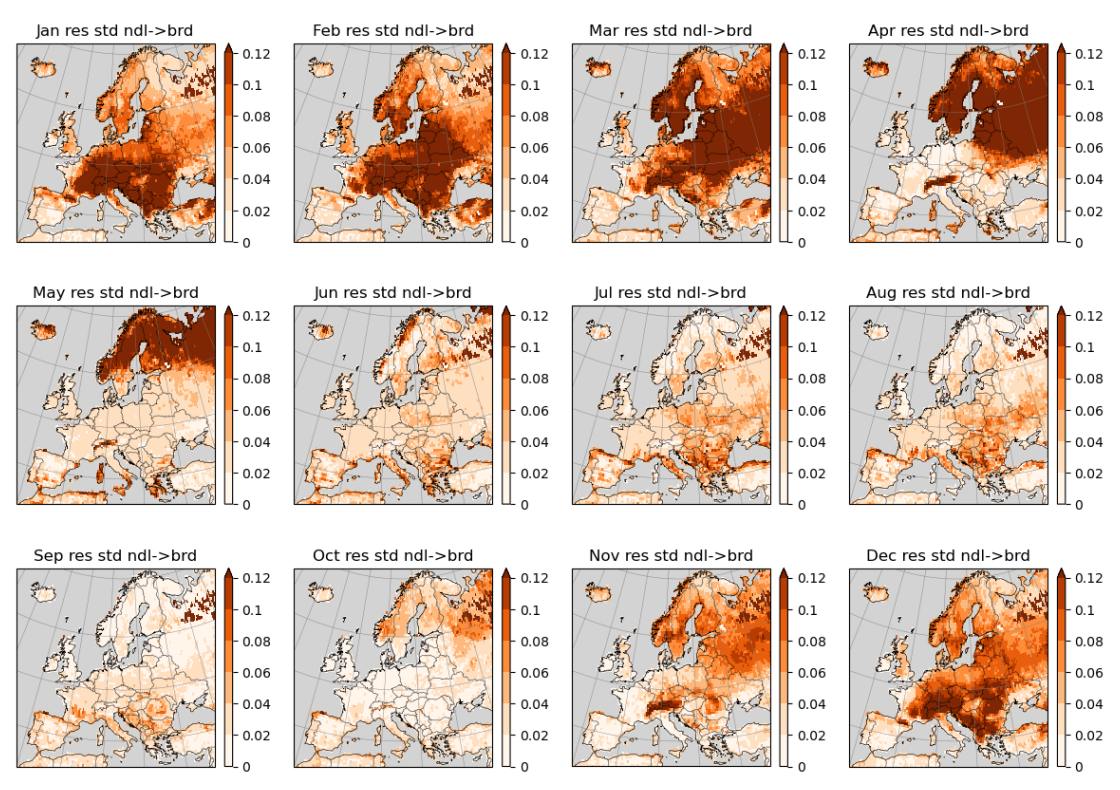


Figure 20. Standard deviation of the residual calculated using the linear relationship between direct biogeophysical impacts of the conversion from coniferous to broadleaf forests on monthly mean daily maximum temperature and the temperature of the grid-cell

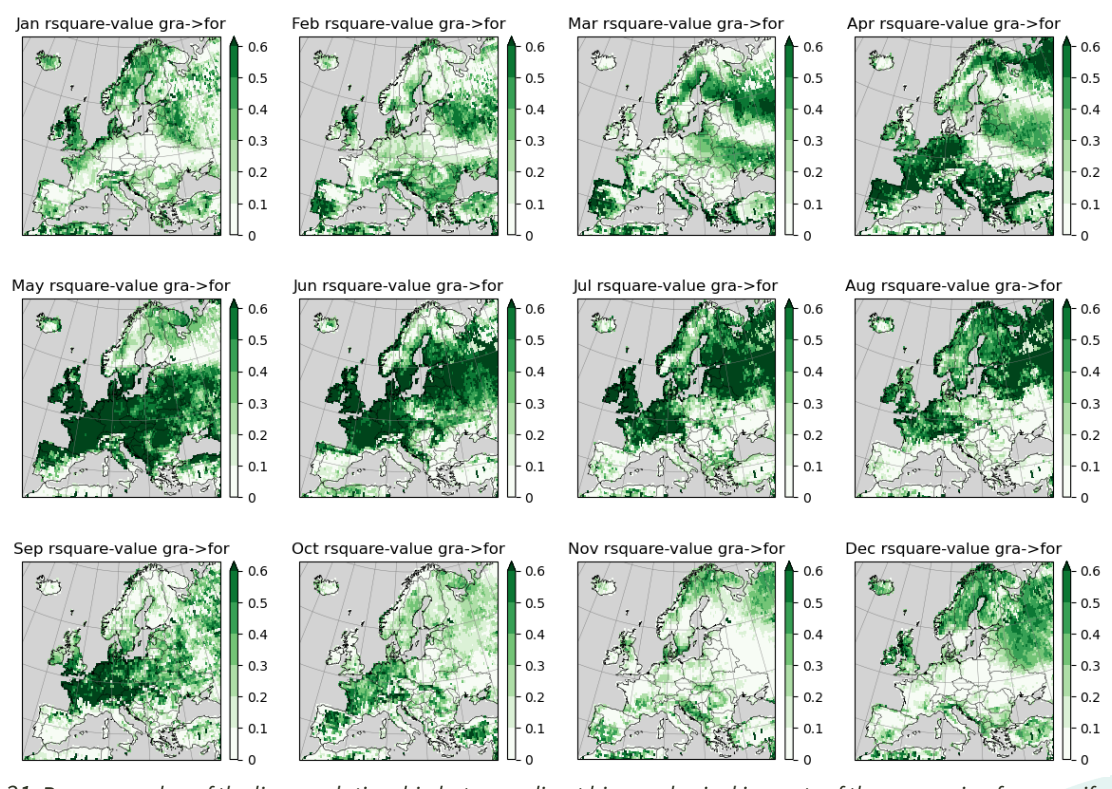


Figure 21. R-square value of the linear relationship between direct biogeophysical impacts of the conversion from coniferous to broadleaf forests on monthly mean daily maximum temperature and the temperature of the grid-cell



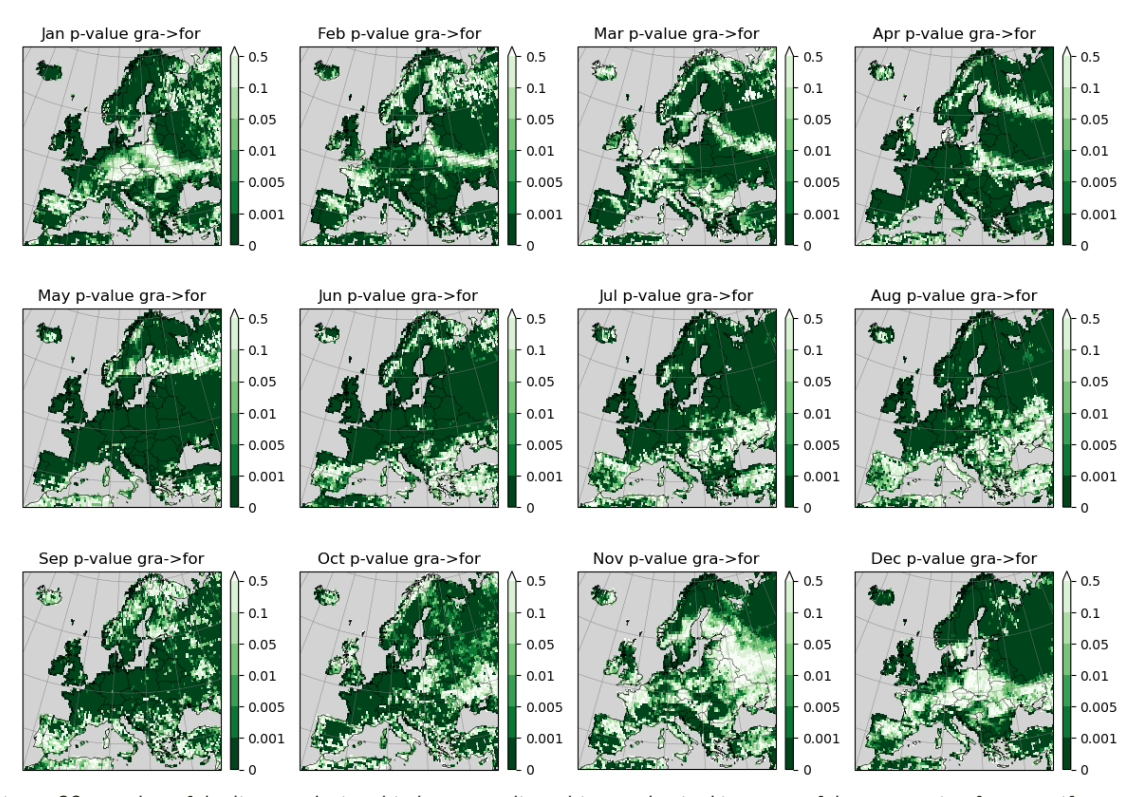


Figure 22. P-value of the linear relationship between direct biogeophysical impacts of the conversion from coniferous to broadleaf forests on monthly mean daily maximum temperature and the temperature of the grid-cell

#### 3.2.4. Conversion to coniferous forests

The slope maps (Figure 23) show widespread positive values from March to August, especially over northern and eastern Europe, indicating that temperature sensitivity increases following the replacement of broadleaf with coniferous cover. This aligns with the known biogeophysical traits of needleleaf forests—lower albedo and higher aerodynamic roughness—which contribute to greater surface warming. Residual standard deviation maps (Figure 24) demonstrate that the emulator struggles most with capturing variability in northeastern Europe during the growing season, where standard deviations peak, possibly due to complex land-atmosphere interactions not fully captured by the linear model. The R-squared values (Figure 25) illustrate strong model explanatory power in summer, especially in high-latitude and central European regions, where values approach or exceed 0.5. This suggests that the emulator effectively captures both the magnitude and variability of temperature changes linked to forest type. Lower R-squared values in western and southern Europe during winter reflect regions where local factors or non-linear feedbacks may play a larger role. P-value maps (Figure 26) confirm that the slope coefficients are statistically significant (p < 0.05) across vast regions during most of the year, particularly from February through September. These results affirm the robustness of the emulator's representation of warming effects due to broadleaf-to-conifer conversion.



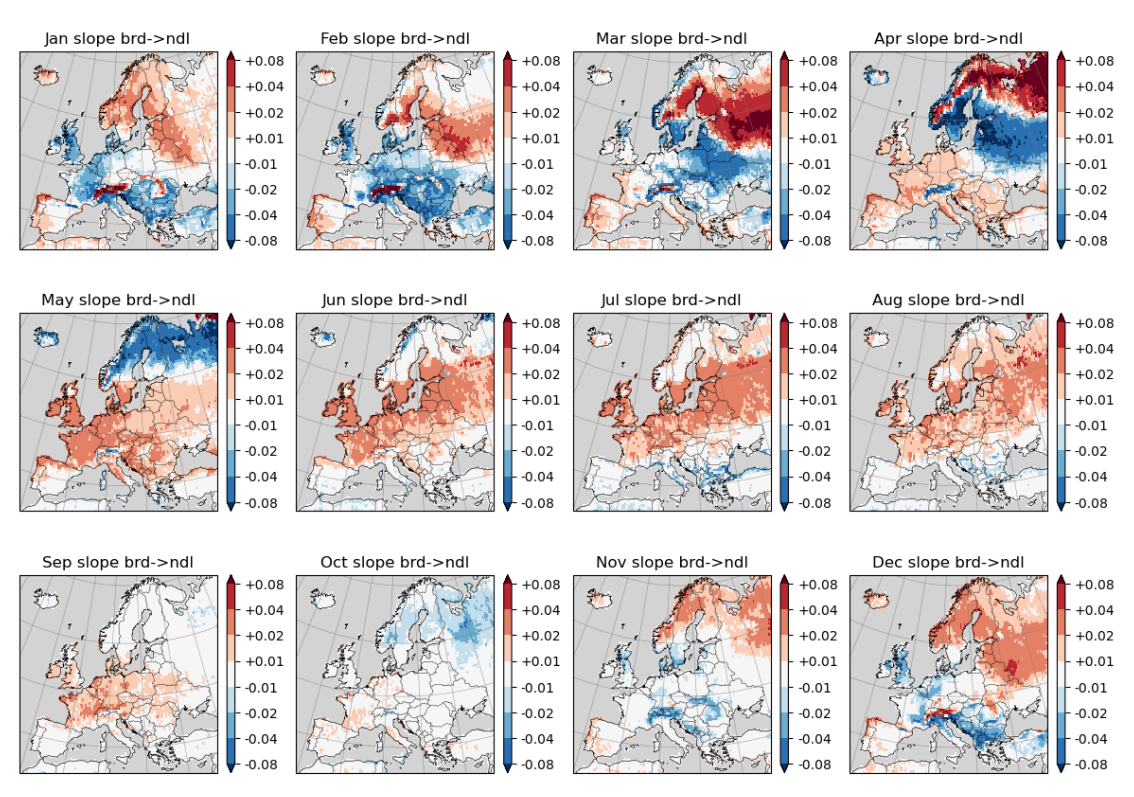


Figure 23. Slope of the linear relationship between direct biogeophysical impacts of the conversion from broadleaf forests to coniferous forests on monthly mean daily maximum temperature and the temperature of the grid cell

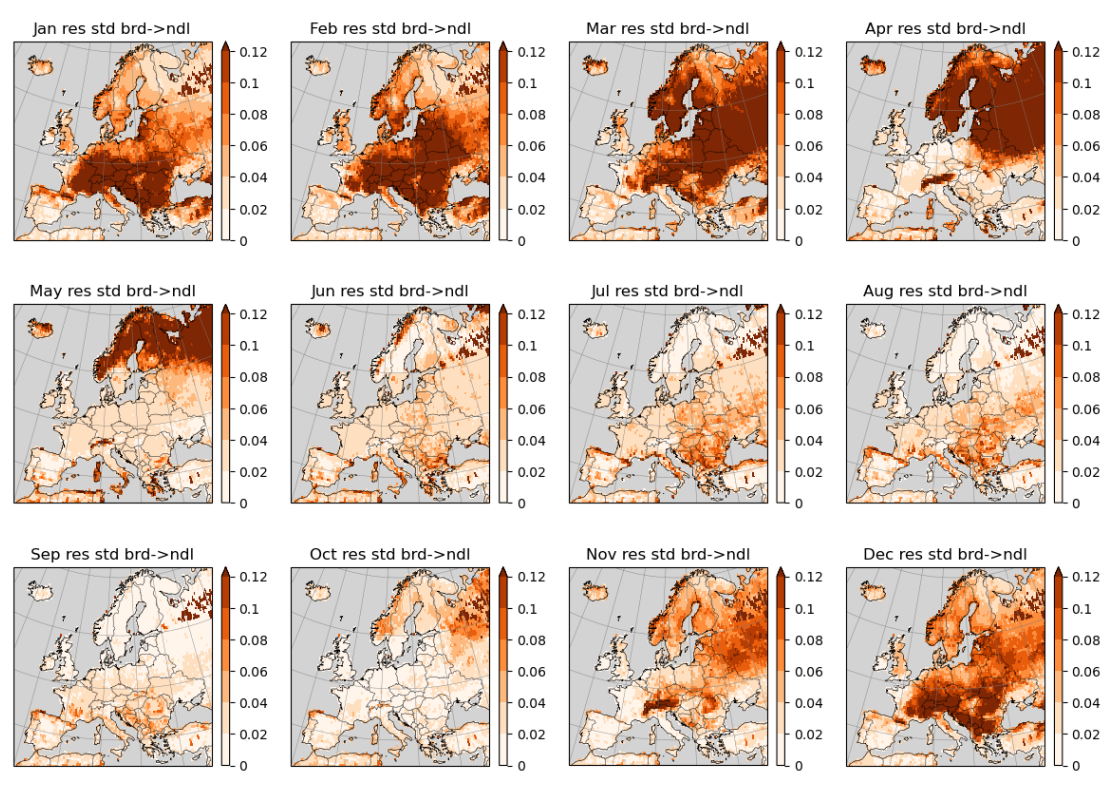


Figure 24. Standard deviation of the residual calculated based on the linear relationship between direct biogeophysical impacts of the conversion from broadleaf to coniferous forests on monthly mean daily maximum temperature and the temperature of the grid cell



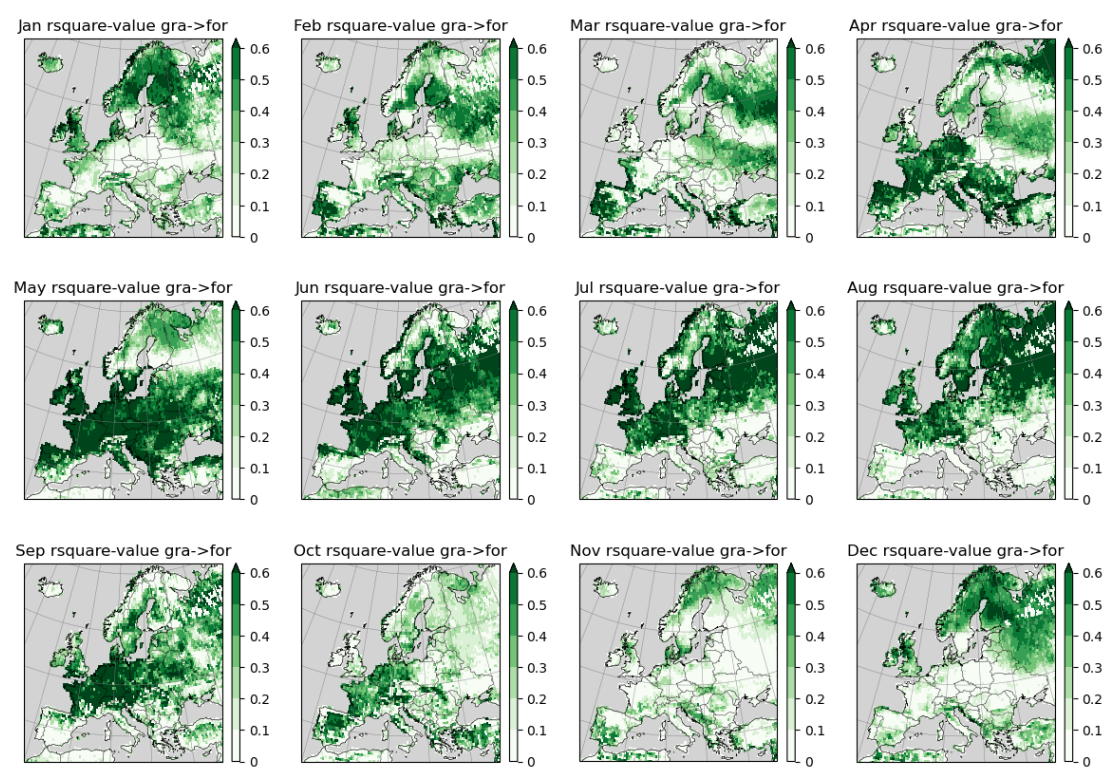


Figure 25. R-square value of the linear relationship between direct biogeophysical impacts of the conversion from broadleaf to coniferous forests on monthly mean daily maximum temperature and the temperature of the grid cell

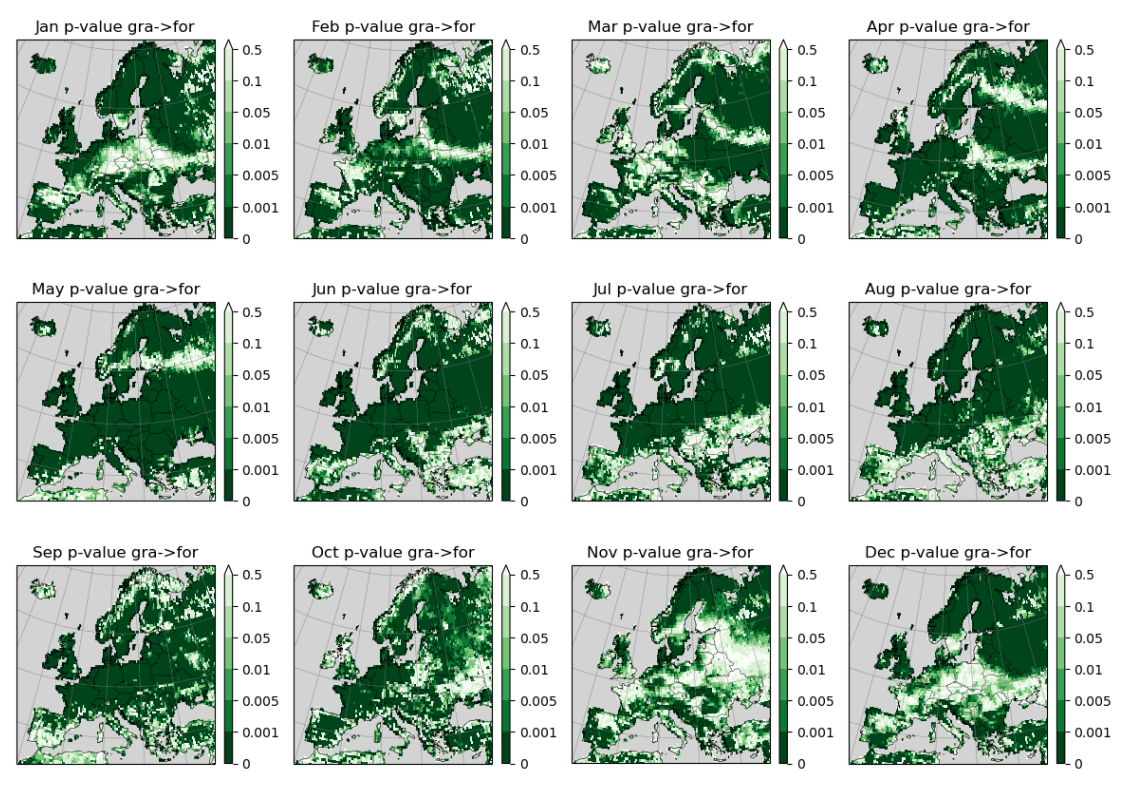


Figure 26. P-value of the linear relationship between direct biogeophysical impacts of the conversion from broadleaf to coniferous forests on monthly mean daily maximum temperature and the temperature of the grid cell



# 4. Challenges and prospects for incorporating ICON-ESM Simulations into MESMER-L-X

The ICON-ESM (Jungclaus et al., 2022) is a comprehensive global Earth System Model. Within the model system, ICON-Land serves as the infrastructural framework for the land component, within which the "Jena Scheme for Biosphere–Atmosphere Coupling in Hamburg", version 4, (JSBACH4; Schneck et al., 2022) is a land surface model responsible for simulating key biogeophysical and biogeochemical land surface processes, including vegetation dynamics, carbon and water cycling, and land-use changes.

Incorporating simulations with ICON-ESM/JSBACH4 into the emulator were met with some challenges, which caused delays, such as ICON-ESM, which is a collaborative effort across several institutions as part of the "National Earth System Modeling Strategy" (natESM), initially still ongoing frequent updates and debugs, missing processes and development requirements and complexities in formulating strategies to fit together the simulations and the requirements for the emulator training data.

Relative to its predecessors, a key advantage of JSBACH4 for forest management modelling is the presence of forest age classes (Nabel et al., 2020), which offer process-level realism to the representation of forest aging. As this feature is unrepresented in COSMO-CLM<sup>2</sup> but could be particularly valuable for an emulator for forest management scenarios, a strategic decision was made to focus the JSBACH4-based emulator component around forestry and associated age effects, while the COSMO-CLM<sup>2</sup> emulator component centers around land cover change as described above.

While it represents an opportunity for more realistic forest management modeling, the aging forest feature introduces considerable complexity into the model simulations' applicability for emulator training. By definition, aging shifts forests continuously through age classes, and this flow cannot be easily paused without extensive manipulation of the model's code and functionality. This understanding led us to identify that a dynamic approach is required: unlike in the COSMO-CLM<sup>2</sup> case, where simple static surface conditions are feasible for emulator training simulations, the JSBACH4 forest age structures are best controlled dynamically through a harvesting process that serves as the model's technical mechanism.

JSBACH4 was however wholly lacking a harvesting process at the beginning of the project, which is why its development has been a significant focus. So far, the development work has established the basic module structure and framework of the process, with the capacity of applying manual harvesting rules in a hard-coded manner. A first version for reading in harvesting input has also been implemented, with functionality to allocate harvesting to input-defined age classes. The current status of the implementation is already sufficient for the generation of idealistic scenarios suited for emulator training, where only immediate biogeophysical impacts are of interest. Future development will further build on this foundation. It will incorporate the handling of varying input use cases (e.g. where harvesting age class is specified and where it is not), as well as internal harvesting rules such as mismatches between input and initial land cover present. Importantly, the current rudimentary harvesting process also merely releases the carbon back into the atmosphere as if the biomass were burned, but the final process will include more realistic carbon and product pools. Ultimately, the finished harvesting process will have the full capacity to run realistic



scenarios based on harvesting input data and will include all the key biogeophysical and biogeochemical surface processes, providing also a realistic carbon cycle.

COSMO-CLM<sup>2</sup> has the benefit of generating sub-grid-level output, and it was decided to take advantage of that capability for extracting direct effects, as outlined earlier. In ICON-ESM, however, fluxes from JSBACH4 are aggregated to the grid cell level, and the atmosphere only observes the total grid cell effect; therefore, no similar sub-grid level output can be accessed as in the COSMO-CLM<sup>2</sup> case. Therefore, extracting both the direct and indirect effects would require a different workaround, such as the method by Winckler et al. (2017), where land cover changes are done selectively in only some grid boxes. An alternative approach to extract the direct effects is to run the offline version of the land component only, i.e., just the land-component JSBACH4 on its own, with the atmosphere only as input. This approach offers the benefit of being computationally efficient and straightforward to implement in the current model status. The offline setup, disallowing atmospheric adjustment or feedback, is a realistic approach to investigate small-scale land cover/land-use changes (which would not affect the boundary layer) and is commonly used as such in the literature (e.g., Duveiller et al., 2018; Forzieri et al., 2018). A limitation, however, is that changes in temperatures higher up, such as the 2-meter air temperature, in response to largerscale vegetation changes are not simulated and could only be approximated with rough assumptions.

For demonstration purposes, Figure 27 and Figure 28 illustrate the model's sensitivity to variations in forest age. The figures present differences in mean monthly surface temperature for each month, based on JSBACH4 standalone (or "offline") simulations under SSP3-7.0 forcing for the years 2041-2053 (using 1979 land cover fraction map). The simulations assume uniform forest age distributions across the land surface. Three forest age conditions are examined: a "young forest" scenario where forest ages range from 27 to 39 years, a "mature forest" scenario with ages from 62 to 74 years, and an "old-growth forest" simulation where the forest age is >150 years. All age ranges correspond to a single age class within JSBACH4's default "increasing spacing" age-class scheme (27–39-year-old forests fall within the 27–55-year age class, and 62–74-year-old forests within the 56–74-year age class, while the oldest tracked age is 150, belonging to the oldest age class of the model). The subplots in each panel show monthly surface temperature differences between mature and young forest simulations (Figure 277), and mature and old-growth forest simulations (Figures 28). The differences are relatively small but not insignificant, especially for monthly mean values (max 0.36°C). There's regional and seasonal variation, as can be expected, depending on where and when latent heat and albedo effects dominate, for example. The differences between mature and old-growth forest (Figure 288) are more subtle, which is not unsurprising, as properties influencing the surface energy balance (e.g., roughness, albedo) differ more between younger forest age groups, where stand structure and canopy closure evolve more quickly. These figures demonstrate that the model captures biogeophysical effects linked to the forest age. However, it should be noted that these land surface temperature differences are not expected to translate to equally significant effects at, for example, 2m air temperature (which could be captured in a coupled model setup, as described before). The 2m air temperature is typically more buffered due to atmospheric mixing and may show considerably smaller differences between forest age scenarios (Winckler et al., 2019). Whether such effects would be significant enough to warrant creating an emulator remains an open question that can ultimately be evaluated only in coupled model runs.

We have identified a couple of strategies for generating training data for an emulator extension capturing forest aging impacts from JSBACH4. The first option involves running simulations similar



to the figures above, where forests age progressively through a single age class over time. This would essentially represent a forest management scenario with a relatively uniform forest structure and a specific rotation length. It would allow linking biogeophysical responses to a single forest age class. However, gathering enough data points would require multiple simulation periods (e.g., Figures 27-28 only covered 13 years), with forest aging needing to restart from zero—or from another experiment—since the current age-class process in JSBACH4 has the technical limitation of not supporting initialization from a selected age distribution. This makes the approach more computationally intensive. A more affordable alternative involves prescribing a uniform forest age distribution, where forest stands are evenly distributed across ages up to a chosen maximum. This would represent a forest management strategy closer to continuous-growth-type management. Such a structure could be continuously maintained through a simulation with a relatively simple harvesting scheme, avoiding the need for repeated simulation runs to capture a single type of management.

An emulator extended with these forest aging effects would require a different approach for the "control" than the COSMO-CLM²-based MESMER-L-X framework, which uses an approximate present-day static land cover distribution as the reference state. Although the control simulation could technically be started from a forest age map generated from existing observation or model-derived forest age structure data, this approach presents complications. Running a dynamically aging control simulation from then on would require an operational "control" harvesting scheme to restrict the evolution of the forest age. Implementing such a scheme would also require a fully completed and operational harvesting process in the model. Therefore, the best approach would be simply having the emulator compare different age schemes to one another (e.g., like in Figures 27 and 28).

The decision of whether and how to extend the emulator to capture forest aging effects should be guided by a cost-benefit evaluation, balancing the possible policy-relevant value with the possible methodological burden. The emulator could be extended with the ICON-ESM/JSBACH4 input, but with a somewhat different methodology for separating direct and indirect effects if the coupled setup is used, and for choosing the control simulation. This would still involve several potentially technically demanding steps, but could be worth pursuing. Extending the emulator based on just the standalone simulations would instead be relatively straightforward but may not yield the full desired climatological insight.



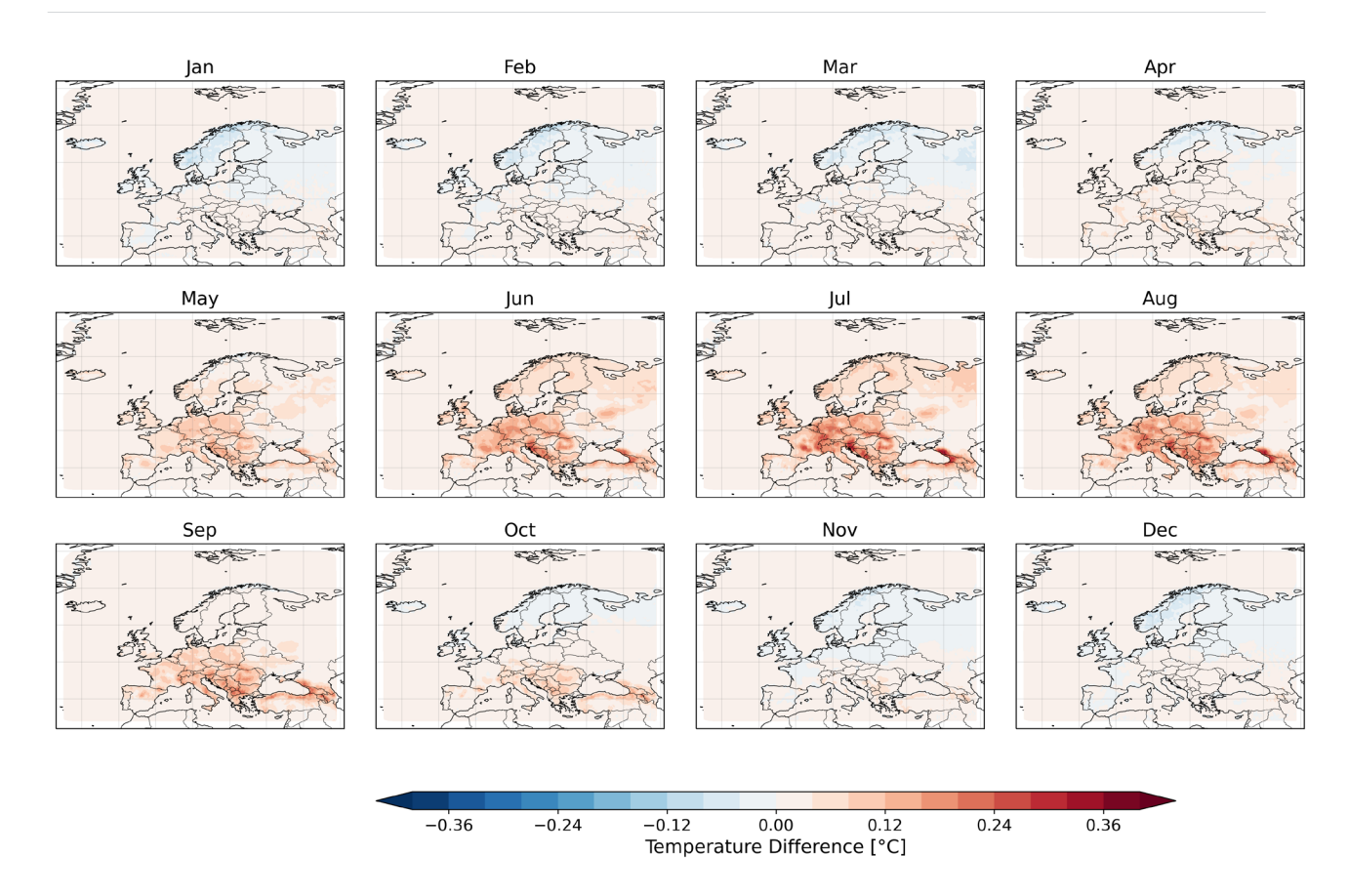


Figure 27. Monthly mean temperature differences between simulations with "young" forests: (27-39 years) and "mature" forests (62-74 years), using the offline land-component JSBACH4. SSP3-7.0: 2041-2053 Climatology

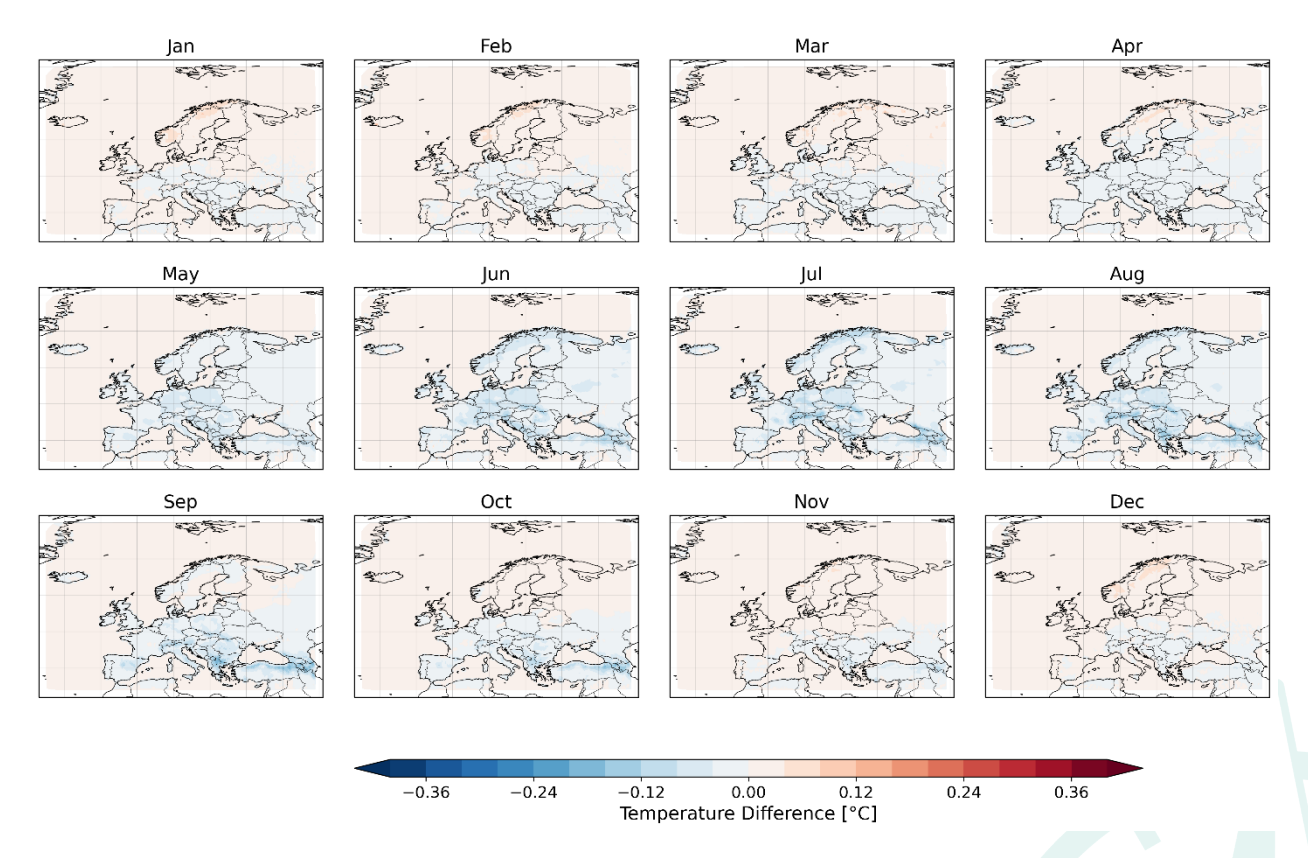


Figure 28. Monthly mean temperature differences between simulations with "old-growth" forests: (>150 years) and "mature" forests (62-74 years), using the offline land-component JSBACH4. SSP3-7.0: 2041-2053 Climatology



# 5. Discussion

In this WP, we first conducted multiple simulations with the regional climate model COSMO-CLM<sup>2</sup> under a warming scenario to assess the biogeophysical impacts of forest changes on near-surface air temperature. Then, based on the outputs from CLM5 at sub-grid level, we separated the direct and indirect impacts on near-surface temperature caused by forest changes. In the end, we developed an emulator, MESMER-L-X, which can reproduce the direct impacts induced by forest change, based on the linear relationship between the background temperature and the direct impacts. This MESMER-L-X is a computationally efficient alternative to traditional climate or Earth system models for assessing the biogeophysical climate feedbacks associated with forest cover and composition changes in Europe.

Results show that afforestation in the majority of Europe can induce a local warming (Figure 3), and this warming effect intensifies with higher temperature in summer months (Figure 11). This is consistent with many previous studies (Davin et al., 2020; De Hertog et al., 2023), which reduces the attractiveness of afforestation in European forest policy. This warming effect is not only limited to the forest land-use tile, but also over other land-use tiles (Figure 4). This indicates that large-scale afforestation may increase the risk of the European population to heat extremes.

One possible solution could be the forest composition change from coniferous to broadleaf forests. This conversion results in net cooling, especially during the growing season and in high-latitude areas, reflecting higher transpiration and surface moisture availability. Conversely, the shift to coniferous forests introduces a marked warming signal, driven by their lower albedo and structural properties that limit evapotranspiration. These findings are consistent with broader literature on forest biogeophysics and support the idea that not all forest cover is climatically equal (Luyssaert et al., 2018; Schwaab et al., 2020).

From a policy perspective, afforestation and reforestation projects should be designed not just for carbon uptake but also for their biogeophysical effects on climate. Promoting broadleaf species in temperate and boreal regions may offer co-benefits by enhancing cooling, whereas extensive conifer planting could inadvertently exacerbate local warming. However, changing the composition of forests may have negative impacts on other aspects of forests, like biodiversity, resilience to wildfire, and local soil water availability, which requires further investigations.

The seasonal and regional variation in slope and intercept parameters confirms that MESMER-L-X captures the direction and magnitude of expected climate responses. Statistically significant relationships, combined with high R-squared values during key periods, especially summer, demonstrate strong predictive performance. However, the emulator's performance is less consistent in winter months and in regions with high residual variability, limiting the confidence to use MESMER-L-X in those months.

In general, the MESMER-L-X emulator is a valuable tool for forest climate policy modeling. By enabling spatially explicit, computationally efficient analysis of land-use-induced climate effects, it bridges the gap between high-resolution process-based models and the practical needs of policy planning. Future work may extend this framework to include feedbacks on precipitation, integrate socioeconomic scenarios, or refine residual components through machine learning techniques, thereby enhancing its scope and accuracy.



Although the ICON-ESM/JSBACH4 simulations were not included in this report, the process described here for the development of the emulator based on COSMO-CLM<sup>2</sup> serves as a proof-of-concept. A somewhat similar approach could also be utilized for a later extension of the emulator with ICON-ESM.

## 6. Conclusion

The MESMER-L-X emulator successfully replicates the direct temperature responses of various forest cover and composition changes across Europe, providing a scalable and scientifically robust tool for supporting forest-related climate policy. Its design—leveraging linear response models with localized variability—ensures both transparency and computational efficiency. The emulator captures key seasonal dynamics, such as summer warming following afforestation and spring cooling associated with broadleaf expansion, aligning with the broader understanding of biogeophysical feedbacks.

These results underscore the importance of accounting for not just carbon fluxes but also biogeophysical processes when designing forest management strategies. MESMER-L-X enables the integration of these feedbacks into policy modelling, scenario analysis, and impact assessment efforts, offering a critical bridge between climate science and decision-making.

Future work should expand MESMER-L-X's scope by introducing a second component for ICON-ESM/JSBACH4 forest with age-associated forest management effects. Later enhancements could include adding interactions with humidity, testing generalizability across other European regions, and incorporating socio-economic data to support broader sustainability and adaptation goals.



# 7. References

Belušić, D., Fuentes-Franco, R., Strandberg, G., & Jukimenko, A. (2019). Afforestation reduces cyclone intensity and precipitation extremes over Europe. Environmental Research Letters, 14(7), 074009.

Beusch, L., Gudmundsson, L., & Seneviratne, S. I. (2020). Emulating Earth system model temperatures with MESMER: from global mean temperature trajectories to grid-point-level realizations on land. Earth System Dynamics, 11(1), 139-159.

Beusch, L., Nicholls, Z., Gudmundsson, L., Hauser, M., Meinshausen, M., & Seneviratne, S. I. (2021). From emission scenarios to spatially resolved projections with a chain of computationally efficient emulators: MAGICC (v7. 5.1)–MESMER (v0. 8.1) coupling. Geoscientific Model Development Discussions, 2021, 1-26.

Davin, E. L., Rechid, D., Breil, M., Cardoso, R. M., Coppola, E., Hoffmann, P., ... & Wulfmeyer, V. (2020). Biogeophysical impacts of forestation in Europe: first results from the LUCAS (Land Use and Climate Across Scales) regional climate model intercomparison. Earth System Dynamics, 11(1), 183-200.

Davin, E. L., Stöckli, R., Jaeger, E. B., Levis, S., & Seneviratne, S. I. (2011). COSMO-CLM 2: a new version of the COSMO-CLM model coupled to the Community Land Model. Climate dynamics, 37, 1889-1907.

De Hertog, S. J., Havermann, F., Vanderkelen, I., Guo, S., Luo, F., Manola, I., ... & Thiery, W. (2022). The biogeophysical effects of idealized land cover and land management changes in Earth system models. Earth System Dynamics Discussions, 2022, 1-53.

Duveiller, G., Forzieri, G., Robertson, E., Li, W., Georgievski, G., Lawrence, P., Wiltshire, A., Ciais, P., Pongratz, J., Sitch, S., Arneth, A., & Cescatti, A. (2018). Biophysics and vegetation cover change: A process-based evaluation framework for confronting land surface models with satellite observations. Earth System Science Data, 10(3), 1265–1279. https://doi.org/10.5194/essd-10-1265-2018

Ellison, D., Pokorný, J., & Wild, M. (2024). Even cooler insights: On the power of forests to (water the Earth and) cool the planet. Global change biology, 30(2), e17195.

Forzieri, G., Duveiller, G., Georgievski, G., Li, W., Robertson, E., Kautz, M., Lawrence, P., Garcia San Martin, L., Anthoni, P., Ciais, P., Pongratz, J., Sitch, S., Wiltshire, A., Arneth, A., & Cescatti, A. (2018). Evaluating the Interplay Between Biophysical Processes and Leaf Area Changes in Land Surface Models. Journal of Advances in Modeling Earth Systems, 10(5), 1102–1126. https://doi.org/10.1002/2018MS001284

Grassi, G., House, J., Dentener, F., Federici, S., den Elzen, M., & Penman, J. (2017). The key role of forests in meeting climate targets requires science for credible mitigation. Nature Climate Change, 7(3), 220-226.



Luyssaert, S., Marie, G., Valade, A., Chen, Y. Y., Njakou Djomo, S., Ryder, J., ... & McGrath, M. J. (2018). Trade-offs in using European forests to meet climate objectives. Nature, 562(7726), 259-262.

Jungclaus, J. H., Lorenz, S. J., Schmidt, H., Brovkin, V., Brüggemann, N., Chegini, F., Crüger, T., De-Vrese, P., Gayler, V., Giorgetta, M. A., Gutjahr, O., Haak, H., Hagemann, S., Hanke, M., Ilyina, T., Korn, P., Kröger, J., Linardakis, L., Mehlmann, C., ... Claussen, M. (2022). The ICON Earth System Model Version 1.0. *Journal of Advances in Modeling Earth Systems*, *14*(4), e2021MS002813. <a href="https://doi.org/10.1029/2021MS002813">https://doi.org/10.1029/2021MS002813</a>

Kirschbaum, M. U. F., Whitehead, D., Dean, S. M., Beets, P. N., Shepherd, J. D., & Ausseil, A. G. (2011). Implications of albedo changes following afforestation on the benefits of forests as carbon sinks. Biogeosciences, 8(12), 3687-3696.

Lawrence, D. M., Fisher, R. A., Koven, C. D., Oleson, K. W., Swenson, S. C., Bonan, G., ... & Zeng, X. (2019). The Community Land Model version 5: Description of new features, benchmarking, and impact of forcing uncertainty. Journal of Advances in Modeling Earth Systems, 11(12), 4245-4287.

Nabel, J. E. M. S., Naudts, K., & Pongratz, J. (2020). Accounting for forest age in the tile-based dynamic global vegetation model JSBACH4 (4.20p7; git feature/forests) – a land surface model for the ICON-ESM. Geoscientific Model Development, 13(1), 185–200. https://doi.org/10.5194/gmd-13-185-2020

Nath, S., Gudmundsson, L., Schwaab, J., Duveiller, G., De Hertog, S. J., Guo, S., ... & Lejeune, Q. (2023). TIMBER v0. 1: a conceptual framework for emulating temperature responses to tree cover change. Geoscientific Model Development, 16(14), 4283-4313.

Nath, S., Lejeune, Q., Beusch, L., Schleussner, C. F., & Seneviratne, S. I. (2021). MESMER-M: an Earth System Model emulator for spatially resolved monthly temperatures. Earth System Dynamics Discussions, 2021, 1-38.

Pongratz, J., Schwingshackl, C., Bultan, S., Obermeier, W., Havermann, F., & Guo, S. (2021). Land Use Effects on Climate: Current State, Recent Progress, and Emerging Topics. *Current Climate Change Reports*, 7(4), 99–120. <a href="https://doi.org/10.1007/s40641-021-00178-y">https://doi.org/10.1007/s40641-021-00178-y</a>

Quilcaille, Y., Gudmundsson, L., & Seneviratne, S. I. (2023). Extending MESMER-X: a spatially resolved Earth system model emulator for fire weather and soil moisture. Earth System Dynamics, 14(6), 1333-1362.

Romppanen, S. (2020). The LULUCF Regulation: the new role of land and forests in the EU climate and policy framework. Journal of Energy & Natural Resources Law, 38(3), 261-287.

Schneck, R., Gayler, V., Nabel, J. E. M. S., Raddatz, T., Reick, C. H., & Schnur, R. (2022). Assessment of JSBACHv4.30 as a land component of ICON-ESM-V1 in comparison to its predecessor JSBACHv3.2 of MPI-ESM1.2. *Geoscientific Model Development*, *15*(22), 8581–8611. <a href="https://doi.org/10.5194/gmd-15-8581-2022">https://doi.org/10.5194/gmd-15-8581-2022</a>



Schwaab, J., Davin, E. L., Bebi, P., Duguay-Tetzlaff, A., Waser, L. T., Haeni, M., & Meier, R. (2020). Increasing the broad-leaved tree fraction in European forests mitigates hot temperature extremes. Scientific reports, 10(1), 14153.

Teuling, A. J., Taylor, C. M., Meirink, J. F., Melsen, L. A., Miralles, D. G., Van Heerwaarden, C. C., ... & de Arellano, J. V. G. (2017). Observational evidence for cloud cover enhancement over western European forests. Nature communications, 8(1), 14065.

Whitehead, D. (2011). Forests as carbon sinks—benefits and consequences. Tree physiology, 31(9), 893-902.

Wieners, K.-H., Giorgetta, M., Jungclaus, J., Reick, C., Esch, M., Bittner, M., Legutke, S., Schupfner, M., Wachsmann, F., Gayler, V., Haak, H., de Vrese, P., Raddatz, T., Mauritsen, T., von Storch, J.-S., Behrens, J., Brovkin, V., Claussen, M., Crueger, T., ... Roeckner, E. (2019). MPI-M MPI-ESM1.2-LR model output prepared for CMIP6 CMIP historical. Earth System Grid Federation. https://doi.org/10.22033/ESGF/CMIP6.6595

Winckler, J., Reick, C. H., & Pongratz, J. (2017). Robust Identification of Local Biogeophysical Effects of Land-Cover Change in a Global Climate Model. Journal of Climate, 30(3), 1159–1176. https://doi.org/10.1175/JCLI-D-16-0067.1

Winckler, J., Lejeune, Q., Reick, C. H., & Pongratz, J. (2018). Nonlocal Effects Dominate the Global Mean Surface Temperature Response to the Biogeophysical Effects of Deforestation. *Geophysical Research Letters*, 46(2), 745–755. <a href="https://doi.org/10.1029/2018GL080211">https://doi.org/10.1029/2018GL080211</a>

Winckler, J., Reick, C. H., Luyssaert, S., Cescatti, A., Stoy, P. C., Lejeune, Q., Raddatz, T., Chlond, A., Heidkamp, M., & Pongratz, J. (2019). Different response of surface temperature and air temperature to deforestation in climate models. Earth System Dynamics, 10(3), 473–484. https://doi.org/10.5194/esd-10-473-2019



### 8. Annexes

### 8.1. Manual of the emulator

The emulator contains a Python class (BGPImpacts (), version Python 3) and several netCDF files containing statistical parameters, which are needed by the emulator. To use the emulator, the users need to download the netCDF files and initialize the class with the directory where the netCDF files are located. The emulator is available here:

https://gitlab.iiasa.ac.at/forestnavigator/wp4/forestnavigator\_d4.3\_mesmer-l-x.git

The use of emulator:

```
bgp = BGPImpacts(base)
```

Where base is the path to the folder.

Then, to calculate the biogeophysical impacts in one grid cell, the compute function needs to be called with multiple mandatory input variables:

```
imp_dir, scaled_imp_dir, rsquared, pvalue = bgp.compute(lat_pt=45.0,
lon_pt=6.0, forchange_type=3, forchange_frac=0.8, month=4,
T_grid=25+273.15, T_type=0, var='TSA')
```

Where input variables include:

lat pt, and lon pt are latitude and longitude of the center point of the grid cell;

**forchange** type is the type of forest change, with six options (

- 1. afforestation (grassland -> forest);
- 2. deforestation (forest -> grassland);
- 3. conversion to broadleaf (coniferous -> broadleaf);
- 4. conversion to needleleaf (broadleaf -> coniferous);
- **5.** afforestation with broadleaf (grassland -> broadleaf);
- **6.** afforestation with coniferous (grassland -> needleleaf));

**forchange frac** is the fraction of the changed area in this grid cell (0-1);

month is the month from January (0) to December (11); T\_grid is the temperature of the grid cell (in K);

T\_type includes monthly mean (0: daily mean; 1: daily maximum; and 2: daily minimum);

var has two values ('TSA': 2-meter air temperature; 'TSKIN': surface temperature).

And output variables are:

imp\_dir: emulated direct impacts induced by forest changes;

scaled\_imp\_dir: imp\_dir scaled over the entire grid cell;



rsquared: R-squared value of the linear relationship trained based on COSMO-CLM<sup>2</sup> simulations;

pvalue: p-value of the linear relationship trained based on COSMO-CLM<sup>2</sup> simulations;

# 8.2. Description of the appendix netCDF files

Several netCDF files with the name starting with Combined\_Stats\_ are provided, which are mandatory if users want to use the emulator. The name of every file can be separated into four parts, representing different information.

Combined\_Stats\_: shared string of all files.

**all\_forest**: the experiment used for the emulator training, together with the control simulation, with six options (see Table 1):

```
all_forest: afforestation;
all_grass: deforestation;
only_forest_broadleaf: conversion from coniferous to broadleaf forests;
only_forest_needleleaf: conversion from broadleaf to coniferous forests;
all_forest_broadleaf: afforestation and the conversion from coniferous to broadleaf forests;
all_forest_needleleaf: afforestation and conversion from broadleaf to coniferous forests;
```

h0-h1 mean: type of the temperature, with three options:

```
ho-h1 mean: monthly mean daily mean temperature;
```

h2-h3 max: monthly mean daily maximum temperature;

h2-h3 min: monthly mean daily minimum temperature;

TSA: the variable of the temperature, with two options:

```
TSA: 2-meter air temperature;
```

**TSKIN**: surface temperature.

In addition to the statistical parameters prepared for the emulator, there are some other variables which may be interesting for users, including

```
control: temperature of the grid cell;
local xx: direct impacts;
```



nonlocal\_xx: indirect impacts.